

# Integrating Micro Process Chemistry into an NMR Spectrometer

Julia Schulte-Hermann, Jing Yang, Andrea C. Hurtado Rivera, Jan G. Korvink, Neil MacKinnon, and Jürgen J. Brandner\*

DOI: 10.1002/cite.202300103

 This is an open access article under the terms of the Creative Commons Attribution License, which permits use, distribution and reproduction in any medium, provided the original work is properly cited.

Miniaturization has proven to be a compelling strategy in many research areas and continuous progress in micro fabrication has contributed to its growing popularity. These advances offer opportunities in analytical characterization technologies. Nuclear magnetic resonance is one such characterization method that has greatly benefited from miniaturization. Many research opportunities remain to be explored, leveraging the advantages of miniaturization in NMR. Here, the benefits of NMR-miniaturization in the fields of micro process engineering, gas-based hyperpolarization, and small-scale bioreactors are reviewed. These applications are discussed in the context of modern micro fabrication approaches and materials, highlighting the most compatible with NMR applications.

**Keywords:** Gas-based hyperpolarization, Micro process engineering, Microfluidic bioreactors, Miniaturization, Nuclear magnetic resonance

*Received:* June 15, 2023; *accepted:* November 02, 2023

## 1 Introduction

Taking advantage of parallelization, cost and space reduction, and process intensification, miniaturization has enabled and continues to facilitate advances in many technological application fields and their associated characterization methods. In recent years, the miniaturization trend has also brought benefits to nuclear magnetic resonance (NMR), with technological advances expanding the application and accessibility of the method. As a non-invasive, non-destructive measurement technology, NMR is compatible with wide range of sample materials and, considering measurement modes including spectroscopy, imaging, diffusion, and relaxometry, this analytical technique offers multiple windows into a sample's structure and dynamics [1]. Material structure revealed by NMR can span multiple length scales, from the 3-dimensional molecular structure (~Angstroms) to complex molecular assemblies (e.g., organism internal structure, ~meters). Dynamics are similarly revealed over a range of time scales, including internal molecular rearrangement (~picoseconds) to molecular transport, and chemical reaction dynamics (~femtoseconds to hours, depending on reaction and process parameters). In this sense, the rich atomic-level information revealed by NMR is unmatched by many other spectroscopic techniques, including infrared, ultraviolet, and Raman. These advantages qualify NMR as highly interesting for a multitude of fields and applications. These wonderful properties do not come for free: drawbacks of NMR include the relatively low measurement sensitivity compared to methods

listed above, and the challenge of experiment and application integration, due to spatial restrictions within the measurement system as indicated in the roughly to scale Fig. 1.

We thus seek to demonstrate the advantages of NMR hardware miniaturization in addressing these drawbacks and highlight the potential of applying NMR to versatile applications in application fields which stand to profit from this information-rich method. To develop an understanding of important factors to consider *en route* to NMR miniaturization, the basic principles of NMR will be introduced, including strategies to improve sensitivity which are often required for miniaturized NMR. Afterwards, the materials compatible with NMR and associated applications will be

<sup>1</sup>Julia Schulte-Hermann  <https://orcid.org/0009-0002-0377-3423>,

<sup>1</sup>Jing Yang  <https://orcid.org/0009-0007-4956-5853>,

<sup>1</sup>Andrea C. Hurtado Rivera

 <https://orcid.org/0000-0001-5307-5928>,

<sup>1</sup>Prof. Dr. Jan G. Korvink

 <https://orcid.org/0000-0003-4354-7295>,

<sup>1</sup>PhD Neil MacKinnon  <https://orcid.org/0000-0002-9362-4845>,

<sup>1,2</sup>Prof. Dr. Jürgen J. Brandner

(juergen.brandner@kit.edu)

<sup>1</sup>Karlsruhe Institute of Technology, Institute of Microstructure Technology, Hermann-von-Helmholtz-Platz 1, 76344 Eggenstein-Leopoldshafen, Germany.

<sup>2</sup>Karlsruhe Institute of Technology, Karlsruhe Nano Micro Facility KNMFi, Hermann-von-Helmholtz-Platz 1, 76344 Eggenstein-Leopoldshafen, Germany.

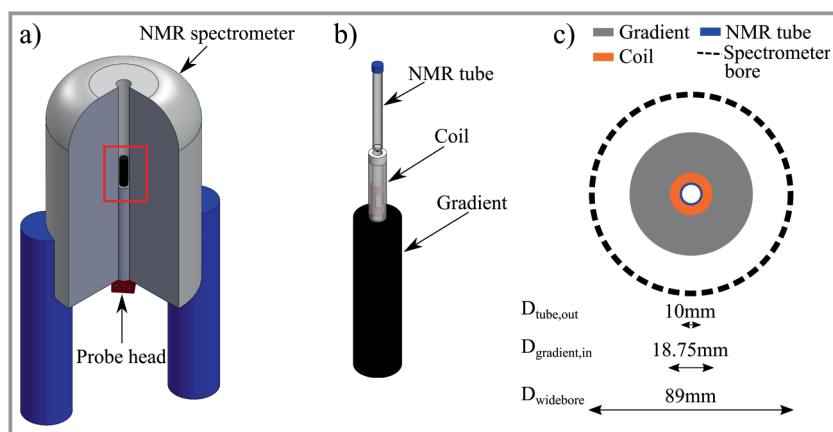


**Figure 1.** Geometrical arrangement of an NMR spectrometer.

introduced, together with microfabrication methods applicable to this sub-class of materials, to show their boundaries and requirements. Finally, a selection of applications highlighting the potential of miniaturized NMR are described, including gas-liquid contactors in the context of gas-based NMR hyperpolarization techniques, miniaturized process engineering devices, and bioreactors with a focus on active metabolism monitoring. In the conclusion and outlook, prospects for future applications are discussed.

## 1.1 Principle of NMR

Atomic nuclei possess the intrinsic property of spin ( $I$ ), the source of magnetization, which can be utilized to reveal detailed sample information including molecular structure, mixture component identities and their quantities, and changes in the molecular content over time (e.g., due to an ensuing chemical reaction). This is possible because nuclei with  $I \neq 0$  possess a magnetic moment whose resonant frequency is exquisitely sensitive to the local magnetic environment. To extract these details, the sample must be immersed in a (typically) strong and uniform magnetic field,  $B_0$ . Given the quantum mechanical nature of spin, the energy states available to the nuclear magnetic moment then split into  $2I + 1$  available states (referred to as Zeeman splitting). In the simplest case of  $I = 1/2$ , two energy states become available, between which transitions can be induced through resonant excitation at a frequency given by  $\omega_0 = -\gamma B_0$ . [1] The local magnetic environment of a nucleus is then sensed as small perturbations to the resonant frequency  $\omega_{local} = -\gamma B_{local}$  with  $B_{local} = B_0(1-\sigma)$ , with details of the local magnetic environment contained with the chemical shielding tensor,  $\sigma$ . NMR enjoys high spectral resolution, so that local magnetic environments with ppb differences in  $\omega_{local}$  can be measured (i.e.,  $\Delta f < 1$  Hz at  $f = \gamma B_0$  MHz resonance frequencies). To induce transitions, and thus measure a signal, we require a population difference between the spin energy states, which brings us to the sensitivity chal-

lenge of NMR: at room temperature and strong magnetic fields (up to 45 T magnetic field strength at time of writing), thermal energy is sufficient such that population differences are on the order of ppm (given ultimately by Boltzmann statistics). For typical commercial NMR systems, this translates to the need for samples containing on the order of  $10^{14}$  identical spins.

Given equilibrium spin polarization, a common strategy to improve sensitivity is therefore to move to stronger  $B_0$  field strengths (methods exploiting non-equilibrium polarization are discussed in Sect. 3.1). Commercial superconducting NMR spectroscopy magnets range from

2–28 T, these powerful magnetic fields bring us to the second challenge, which is experiment integration inside the magnet. The materials chosen to extend the applicability of NMR must be compliant with application immersion in a strong magnetic field, both from a safety standpoint, and to ensure that the spectral quality of the NMR measurement (i.e., high resolution) is not compromised.

NMR hardware miniaturization has the potential to both improve sensitivity and enable NMR measurement of experiments featuring increased sophistication (selected examples are discussed in Sect. 3). Developments in the field of miniaturized NMR hardware began with the radiofrequency (RF) coils, an essential NMR hardware component responsible for both broadcasting RF power to the sample for excitation and receiving the signal from the excited system. Microcoil probe head technology has become a powerful tool to enhance the mass-sensitivity of NMR measurements, optimized by discovering the correct coil geometry for a specific application. A rich variety of approaches and applications have been reported and are detailed in numerous reviews [2–7]. Korvink et al. [8] have discussed the advantages that miniaturized NMR can offer to the experimentalist, extending beyond RF coil miniaturization and considering the magnet, spectroscopy control electronics, and gradient systems.

## 2 Materials and Manufacturing Methods

The ever-increasing miniaturization of systems has been possible to a great extent due to breakthroughs by the MEMS community in suitable manufacturing methods. For NMR-related applications, the development of devices is challenging due to safety and compatibility aspects. In this section, criteria for material selection will be explained, and a selection of materials compatible with NMR will be highlighted. Afterwards, manufacturing methods capable of achieving the needed resolution for miniaturized devices using this sub-class of materials will be reviewed.

## 2.1 Materials

The optimal material selection for the manufacturing of micro devices that targeting an NMR environment is a challenging task, as the materials must simultaneously fulfill several requirements in order to guarantee safe operation and accuracy of measurements. The first aspect to be considered is the possible interaction between the strong magnetic field and the magnetic properties of the material, which can result in translational forces and torques. In order to be able to assess this, an understanding of the fundamental properties of materials is needed. Erhardt et al. [9] described the influence of different materials and physical effects that arise upon insertion of an electrical device into MRI spectrometer.

Materials can be classified according to their magnetic properties as diamagnetic, paramagnetic, ferromagnetic, antiferromagnetic, or ferromagnetic [10]. The most relevant for the present article are diamagnetism, in which the magnetic field is weakened inside the material, paramagnetism, in which the magnetic field is enhanced inside of the material, and ferromagnetism, in which the magnetic field is enhanced inside of the material and the magnetic moments are mutually aligned. More detailed information can be found in the literature [10,11]. For safety reasons, ferromagnetic materials are not used for devices within or in the vicinity of the magnet, as they experience large translational forces when exposed to magnetic field gradients, and torques when exposed to a magnetic field gradient, both of which can result in hazardous situations [12]. The forces exerted on paramagnetic and diamagnetic materials with a magnetic susceptibility on the order of  $\sim 10^{-5}$  can be considered negligible, so these materials may be generally used in NMR setups [9].

The magnetic susceptibility of a material and, more precisely, the interface between materials with different magnetic susceptibilities in the vicinity of where the MR signal is detected, must be carefully considered [13]. Failure to 'susceptibility match' material interfaces will create local distortions in the magnetic field, modifying the local field  $B_{local}$  with an additional term dependent on the distance from the interface. If in the sample vicinity,  $\omega_{local}$  is concomitantly modified resulting in observed signal broadening in NMR spectroscopy and, in the case of imaging, inaccuracies in shape and/or position of MR images or versatile image artifacts [14]. The magnetic susceptibility is influenced by the material composition, however, other physical parameters, such as surface roughness and shape, can also distort the magnetic field homogeneity, for which reason it is important to consider these when designing a device. A very thorough and detailed study of different materials' magnetic susceptibility was performed by Wapler and co-workers [15].

The second aspect that must be considered is the electrical conductivity of a material. As described by Faraday's law of induction, any change in the magnetic field will induce a

current in electrically conductive materials. This induced electrical current can lead to heating, forces, and distortions in the magnetic field, which will in return deteriorate the MR signal. In poorly designed cases, conductive materials completely shield the sample from the excitation signal and effectively eliminate the MR signal.

Lastly, the materials selected must robustly satisfy the demands of the process they will be used for, such as temperature, chemical inertness, gas-tightness, and mechanical strength for withstanding applied pressure forces. Whilst selecting the material, not only the previously mentioned criteria must be taken into account, but also the manufacturing methods compatible for each material and their spatial resolution. In the following, several materials and their compatibility with NMR, as well as their suitability for chemical engineering devices, will be explored. The manufacturing methods will be the focus of the next section.

A material family commonly used in the field of NMR are glasses, most commercial NMR tubes are made of borosilicate glass 3.3, and in some cases, of quartz. Glasses have excellent thermal and chemical resistance and keep their mechanical strength over a higher temperature range in comparison to other materials. Specific values depend on the manufacturer and manufacturing method, but as an example, Duran borosilicate glass 3.3 from Schott can withstand temperatures of up to 525 °C [16]. Due to their brittle nature, special attention needs to be paid to device handling and possible crack propagation. The use of glass for micro process engineering devices, such as micro reactors, mixers, heat exchangers, and bio reactors, has extensively been reviewed in the literature [17–19].

Wapler et al. [15] observed a large variation of susceptibilities for different glass types, which the authors attributed in some cases to a relatively high iron content. However, it is possible to fine-tune the magnetic susceptibility of glass to match that of the solvent. This was done by Takeda et al. [20], who used a magnetic susceptibility-matched glass and a slot shape for the sample cavity, which allowed for a better signal-to-noise ratio (SNR) in comparison to traditional NMR tubes.

Ceramics, specifically technical ceramics, have excellent mechanical properties, are temperature and corrosion resistant, and chemically inert. Typical melting points are 1850 °C for silicon nitride, 2054 °C for aluminum oxide, and 2710 °C for zirconium dioxide [21]. This makes them a very good match for chemical process engineering applications in which any of these properties are needed. Different ceramics have already been used for micro devices in the area of process engineering and bio engineering, proving their suitability for these fields [22–24]. Furthermore, the suitability of aluminum oxide and zirconium oxide has been proven for high-resolution NMR spectroscopy [25, 26].

Polymers are also often used in the field of NMR. The wide selection of materials within this group has properties that vary greatly, such as mechanical strength, corrosion resistance and chemical compatibility. The temperature

resistance of polymers is lower than that of ceramics and glasses, however, some can withstand relatively high temperatures, such as polyether ether ketone (PEEK) (250 °C) [27] and polytetrafluoroethylene (PTFE) (260 °C) [10]. PTFE, being halogenated, has a low  $^1\text{H}$ NMR background (the most commonly measured nucleus), however, due to the difference in magnetic susceptibility, it can induce artifacts [15]. Polymers, such as polydimethylsiloxane (PDMS) and poly(methyl methacrylate) (PMMA), are also applied in bio-medical applications. These two polymers are regularly used for microfluidic bioreactors [28]. Most polymers are electrical insulators, which makes them suitable for NMR applications. Furthermore, most are relatively cheap, and are compatible with many manufacturing methods, such as additive manufacturing, machining, or molding.

The vast polymer library can be reduced to a smaller selection when considering the need for magnetic susceptibility matching, chemical permeability requirements, and minimal background NMR signal contribution. As an example PDMS is a well-known polymer in microfluidic applications, in the context of NMR devices, one must be aware of the large proton content and relative softness of the polymer, translating into undesirable  $^1\text{H}$ NMR background signals [15]. PDMS is also permeable to gases, and thus a poor choice for perfectly sealed devices, but advantageous when gas-solution contacting is desired (as discussed in Sect. 3.1). Wapler et al. [15] studied a variety of polymers and identified polyurethane (PU) and PMMA as good alternatives to PDMS. The magnetic susceptibility of PU and PMMA is much closer to that of water (a common solvent for NMR samples) than is the case for PDMS, and together with a strongly reduced  $^1\text{H}$  signal ( $10^{-3}$  smaller in the case of PU) these polymers are attractive substitutes.

## 2.2 Manufacturing Methods

In recent years, new 3D manufacturing methods have been established, and existing manufacturing methods have been improved, so that also higher spatial resolutions can be achieved. These new or improved methods have also been extended for materials that are otherwise not easily machined. A manufacturing category which has seen many breakthroughs recently is additive manufacturing. Several different techniques can be allocated to this category, their common trait is the layer-wise manner in which the parts are created. Additive manufacturing methods can, in many cases, be manufactured to achieve more complex geometries than other traditional manufacturing methods. Furthermore, they allow for relatively quick manufacturing of parts starting from a CAD model, which shortens development times.

One method often used within this family is stereo lithography (SLA). In this process, a liquid photo curable resin housed in a vat is sequentially exposed to a patterned light source, typically a collimated UV light beam, or laser, in

order to build sequential solid material layers. The layers adhere to a moveable platform. When the platform is driven downwards into the vat, close to a non-adherent transparent membrane that separates the light source and the resin, a new layer is cured by means of the light source. The platform then moves away from the membrane, and again downwards into the vat, allowing for replenishment of and subsequent curing of the next thin polymer layer. This process repeats itself until an entire object is manufactured [29]. Depending on the resin and the design of the part, different post processing steps are required, such as removing of support structures, washing and curing. The achievable resolution depends on the printer and material, [30] and can be as small as 5 to 10  $\mu\text{m}$  in width and 10  $\mu\text{m}$  in layer thickness [31] in some systems. A challenge of this method is the removal of uncured resin after printing, which, depending on the geometry, can prove rather difficult [30]. In this sense, inner cavities are not possible without an outlet through which the uncured resin can be evacuated. Furthermore, the material choice when working with SLA is limited to photo curable polymer resins [29].

Significant effort has been devoted to extending SLA beyond polymer-based resins. A recent breakthrough in this field is that of Kotz et al. [32], who have developed a photo curable silica nanocomposite compatible with benchtop stereo lithography printers. The resin consists of amorphous silica nanoparticles in a monomeric matrix. Parts manufactured with this resin must be subsequently thermally treated in order to remove the monomer and obtain pure glass parts through nanoparticle sintering. The authors achieved a resolution of a few tens of micrometers, and the resulting glass parts are fully amorphous, non-porous, and have a surface roughness of a few nanometers. A glass part obtained with the developed resin and stereo lithography can be seen in Fig. 2a.

Another technique within the category of additive manufacturing is lithography-based ceramic manufacturing (LCM), which has been developed for ceramic microparticle feed stocks. This technique is similar to SLA printing: the layers are built sequentially on a moveable platform through curing by a light engine [33, 34]. The slurries consist mostly of photo curable monomers and ceramic particles, therefore, thermal post processing, namely debinding and sintering, is needed after printing in order to remove the polymer to obtain a dense ceramic part. With the newest machines, resolutions down to 25  $\mu\text{m}$  are achievable for the green body [35], which is the state of a part before debinding and sintering, consisting of ceramic material embedded in a polymer matrix.

As discussed in Sect. 2.1, ceramics are very well suited for chemical process engineering devices in NMR setups, however, they are very challenging to manufacture, especially when complex and/or 3D geometries are needed. LCM allows for complex geometries, as seen in Fig. 2b, which depicts a cellular cube, and Fig. 2c, which shows a heat exchanger with an inner diameter of 10 mm. Several materials

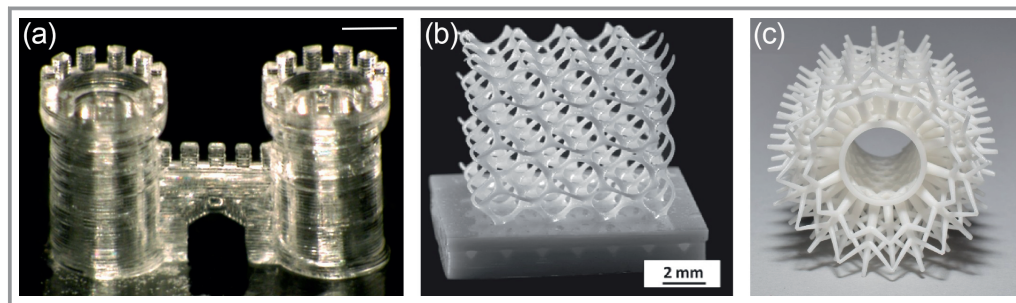


**Figure 2.** Parts fabricated with the additive manufacturing method stereo lithography. a) Glass castle gate from Kotz et al. [32] (scale bar 270  $\mu\text{m}$ ), © 2018 Springer. b) Aluminum oxide cube from Schwentenwein et al. [34], reprinted with permission from the American Ceramic Society © 2015. c) Aluminum oxide micro heat exchanger (inner diameter 10 mm) from Scheithauer et al. [38], © 2018, Springer.

have been demonstrated, including aluminum oxide, zirconia, and silicon nitride [36]. A challenge of this technology is achieving channels with high aspect ratios, as the slurry remaining within the channels needs to be removed. The applicability of this manufacturing method has been shown for microreactors [37] and micro heat exchangers [38].

Direct laser writing (DLW) represents another important advance in additive manufacturing techniques, based on the principle of two-photon absorption. Here, a femtosecond laser is used to structure a photosensitive resin [39, 40]. The achievable resolution depends on the device and resin used, with some systems achieving 100 nm [41]. Until now, the application of this technique to devices in the field of chemical engineering had been limited by the available materials. However, most recently, a resin for manufacturing of glass microstructures compatible with this technique has been developed by Kotz et al. [42]. The authors achieved resolutions of tens of micrometers, with a surface roughness of 6 nm.

In contrast to the newer additive manufacturing methods, some subtractive methods have long been established as the norm in the field of micro systems technology, such as laser cutting and rastering. In this process, a highly focused high-power laser is used to melt and evaporate material in the beam focus. Beam intensity can be used to regulate how much material is subtracted, so that the laser can cut through or only down to a specific depth [43]. The manufacturing resolution for laser cutting and ablation is above 25  $\mu\text{m}$  [44] and is highly dependent on the laser focus which determines the cutting depth and width [45]. In general, this fabrication method offers a high processing speed and quality [45]. Furthermore, it is cast and mold free and suitable for mass production [44]. Nevertheless, surface roughness and irregular profiles commonly occur with the method, which can be minimized by adjusting the fabrication parameters of the laser cutting device [44] or by post-processing methods.

Subtractive etching processes are commonly used in the micro systems field. They work on the principle of transporting an etchant to a surface, which react together, and afterwards removing the reaction product from the surface

[46]. To achieve structures and geometries with etching processes, masks need to be applied onto the surface to locally restrict the etching process. The masks can be manufactured or applied through photolithography, laser beam writing, or other similar methods. Depending on the etchant, the process can differ between isotropic or anisotropic etching [47]. Additionally, the etching processes can be divided into wet and dry etching methods.

Wet etching is a versatile fabrication method which is used to micro fabricate a variety of structures. After the application of the mask onto the sample, the sample is placed into the etching solution with temperature control and stirring functions [47]. Possible etch solutions are for example, HNA solutions, which are a mixture of hydrofluoric, nitric, and acetic acids or alkali-hydroxide etching solutions [47]. Dependent on the chosen etch solution and mask application the pattern resolution can be as small as 12 to 15 nm as Tiron et al. [48] have demonstrated.

Wet etching is a versatile fabrication method which is used to micro fabricate a variety of structures. After the application of the mask onto the sample, the sample is placed into the etching solution with temperature control and stirring functions [47]. Possible etch solutions are for example, HNA solutions, which are a mixture of hydrofluoric, nitric, and acetic acids or alkali-hydroxide etching solutions [47]. Dependent on the chosen etch solution and mask application the pattern resolution can be as small as 12 to 15 nm as Tiron et al. [48] have demonstrated.

As stated by Madou, [46] “dry etching covers a family of methods by which a solid state surface is etched in the gas phase, physically by ion bombardment, chemically by a chemical reaction with a reactive species”. Some methods of dry etching are ion etching, ion beam etching, or reactive ion etching, to name a few example [47]. For dry etching, the manufactured geometries are dependent on the chosen etch technique, etch rate, and mask application techniques. The pattern resolution can go down to 11 nm with aspect ratios up to 20 [49].

In addition to additive and subtractive methods, forming methods are also commonly used. One such method is soft lithography molding. In this casting technique, a pattern is

created through lithography in a thin film immobilized on a silicon wafer. Afterwards, PDMS pre-polymer, or any similar material, can be poured into the mold and cured. The cured part can then be removed and used for the planned application. Depending on the exact soft lithography method, the resolution can be as low as 10 nm [50]. One of the main advantages of this fabrication method is that one mold can be used repeatedly to produce numerous replicas, which reduces manufacturing time and cost [50]. On the other hand, the limitation of material choice can lead to disadvantages. PDMS, one of the most frequently used materials with this method, can shrink by a factor of circa 1 % during curing, which can have a high impact on microstructure quality [50], and swelling can occur in contact with non-polar solvents [51]. More common disadvantages are the inaccuracies of a part due to deformation of the elastomers, and problems in achieving accurate registration of the transparent materials [50]. The manufacturing of a microfluidic bioreactor by means of soft lithography has been shown in previous studies [52–54].

Hot embossing is a forming method with increased popularity for microfabrication. A polymer substrate is heated above its glass temperature and then shaped by pressing a mold insert with constant force into its surface. After cooling, the mold is removed and the now formed substrate can be directly used [55]. A schematic of the process is given in Fig. 3. Hot embossing can be classified in two variants, conventional or single-stage, and roll-to-roll [56]. The process is well suited for high quantities. The mold can consist of different materials, such as silicon or nickel coated metals, and substrate material variants can be a variety of polymers and even glass [55]. Depending on the substrate material used, and the hot embossing technique, the resolution can be as precise as 50 nm [57]. Hot embossing offers an easy and inexpensive method for production, with high throughput and high accuracy [55]. However, one of the main challenges is evaluating of the optimal process parameters, such as the applied force, speed, and temperature, as they directly influence the accuracy of the manufactured part [55].

Injection molding is most commonly used for forming polymers [47], but has also been employed for some metals, such as stainless steels [59]. For injection molding, the material is heated and melted in the plasticization zone of

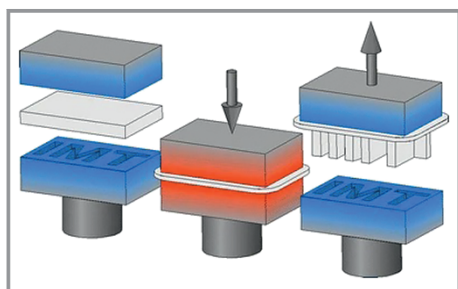


**Figure 3.** Hot embossing process, reprinted with permission from Worgull et al. [58], © 2008, Springer.

the injection unit, while being transported forward with a screw. Subsequently, it is injected into the mold and cooled down. After solidification, the mold can be opened, and the finished part can be removed [47]. The dimensions of produced structures and parts depend on the mold design, the applied subclass of microinjection molding, the process parameters, and the chosen materials [60]. Gibos et al. [61] provide a good overview of the different manufacturing processes of the molds and their tolerances and dimensions. Dimensions of 100  $\mu\text{m}$  for structures are reported as the current limiting resolution [59, 60].

### 3 Select Applications

NMR has a long tradition in chemical engineering, and its usefulness has been well documented. The field is undergoing a trend towards miniaturization, which not only enables higher heat and mass transfer rates, but also higher control over process parameters and novel process window [62]. This new category – micro chemical engineering – can greatly benefit from the advantages of NMR as an analytical method. By MR spectroscopy, chemical detail of reactions occurring within micro reactors, or cell metabolism within a microfluidic bioreactor, can be revealed, while MR imaging can map the components, temperature, and velocity distribution within micro mixers, among many other possibilities. Conversely, micro devices can help bridge NMR limitations when smartly implemented into a given setup, for example by performing mixing with short time constants immediately before the acquisition volume, by enabling new techniques such as gas-assisted hyperpolarization to improve sensitivity, or by integrating additional functionality to enable additional degrees of experimental freedom. These examples and many others will be explained in detail in the following sections. The applications have been broadly divided into gas-liquid contactors (specifically for hyperpolarization), chemical process engineering, and metabolism monitoring and detection through microfluidic platforms and bioreactors. The most prominent papers reviewed in this article can be found in Tab. 1.

#### 3.1 Gas-Liquid Contactors Used in Hyperpolarized NMR Technology

The dominant limitation of NMR spectroscopy is its relatively low sensitivity, caused by the tiny population difference between the spin energy states. Many strategies have been utilized to overcome this inherent impediment and achieve sensitivity enhancement in terms of hardware (stronger magnet, cryo-cooling probe, and microcoil) and software (optimized pulse sequence for acquisition and signal averaging). In addition, gas-based hyperpolarization (spin exchange by optical pumping – SEOP, and parahydrogen induced polarization – PHIP) have emerged as promis-

**Table 1.** Summary of application papers reviewed in this article.

Author	Device	Application
Ahola et al. [113]	Interdigital glass micro mixer & Determination of flow velocity distribution	Determination of flow velocity distribution
Tozzi et al. [110]	Split and Recombine (SAR) mixer	Experimental study of multi-lamination of a non-Newtonian fluid
Lim et al. [114]	Split and Recombine (SAR) mixer	Experimental study of multi-lamination of a non-Newtonian fluid
Mihailova et al. [111]	MX mixer	Study of laminar mixing of Newtonian and non-Newtonian fluids
Herold et al. [112]	SMX mixer	Determination of flow velocity distribution of non-Newtonian fluid
Wiese et al. [115]	Staggered herringbone micro mixer (SHM)	Determination of flow velocity distribution
Bornemann et al. [117]	NMR flow cell with integrated micro mixer	NMR quantitative study of fast chemical reactions
Plata et al. [116]	Micro fluidic chip	Operando study of serial mixing experiments in microliter range
Ulpts et al. [119]	Reactor	Operando study of ethylene hydrogenation with different catalysts
Brächer et al. [121]	Thermostatted micro reactor with integrated micro mixer	Monitoring of reactions with short time constants at a given temperature
Tijssen et al. [118]	Micro reactor with micro fluidic line	In-line analysis of heterogeneous catalysis under elevated pressure
Sesti et al. [120]	Zirconia reactor	Study of CO <sub>2</sub> sequestration in minerals at elevated temperatures and pressure
Hurtado Rivera et al. [123]	Micro heat exchanger	Control of reaction temperature for operando analysis of reactions
Baumer et al. [94]	Hollow fiber membrane contactor	Dissolution of <sup>129</sup> Xe in H <sub>2</sub> O, DMSO and bioliquid
Amor et al. [100]	Hollow fiber membrane contactor	Dissolution HP <sup>129</sup> Xe in porcine blood
Cleveland et al. [101]	Hollow polypropylene fibre membrane contactor	Quantitative MRI and NMR analysis of dissolution efficiency of HP <sup>129</sup> Xe in blood
Amor et al. [95]	Hollow fibre membrane contactor	Infusion of HP <sup>129</sup> Xe in flowing aqueous solution
Roth et al. [96]	Hollow fibre membrane contactor	Parahydrogenation of 2-hydroxyethyl acrylate in D <sub>2</sub> O
Lehmkuhl et al. [84]	PEO-PBT (Poly(ethylene oxide)-poly(butylene terephthalate)) copolymer flat membrane contactor	Investigation of SABRE hyperpolarization under different flow conditions
Bordonali et al. [97]	PDMS flat membrane contactor	Chemosensing of high field SABRE hyperpolarization
Eills et al. [98]	PDMS Flat membrane contactor	Quantitative study of hydrogenation kinetics by PHIP
Tomhon et al. [99]	Tube-in-tube contactor with AF2400 membrane	Continuous hyperpolarization of pyridine and pyrazine by SABRE
Mehendale et al. [134]	Capillary system NMR platform	Metabolic monitoring of bioprocesses
Hertig et al. [136]	NMR tube bioreactor with collagen-based 3D cell culture	Observation of cellular metabolism and mitochondrial respiration
Alshamleh et al. [137]	NMR tube bioreactor containing cell friendly matrix	Monitoring metabolism of acute myeloid leukemia cells
Xue et al. [135]	Controlled bioreactor with automated NMR insert	Monitoring metabolic pathways of Moorella thermoacetica
Yilmaz et al. [139]	Sealable in-situ perfusion NMR bioreactor	Characterisation of oxygen permeation for cell cultures
Patra et al. [140]	In-situ NMR cell growth and monitoring chip	Non-invasive monitoring of a single cancer spheroid

ing approaches to boost the NMR signal intensity and extended the scope of the NMR spectroscopy.

This section will first briefly introduce SEOP and PHIP to put the ensuing discussion into context. Then the challenges in delivering hyperpolarized gas species in liquid-state NMR, and how these challenges may be addressed, is discussed. Finally, various devices implemented in the literature to deliver the hyperpolarized gas substances into bulk or microscale solutions are described and discussed.

Hyperpolarization methods based on gaseous species (SEOP and PHIP) exhibit enormous potential by taking advantage of the following aspects: firstly, hyperpolarized gas can be easily extracted and purified from the mediating substance of the hyperpolarization process; secondly, hyperpolarized gas dissolves in specific solutions allowing novel applications in biosensing or MRI contrast agent development. Several studies utilized optically hyperpolarized gas in pure gaseous form for investigating the pulmonary functions of human lungs [63–65]. Furthermore, gas dissolved in many bio-liquids enables direct observation of the metabolic processes and can help probe the structure of low concentration biomolecules [66–70]. Approaches exploiting PHIP and its sub-class SABRE (signal amplification by reversible exchange) are also promising because of the readily accessible instrumentation (Earth's magnetic field) and short detection time of enormously polarized signals (from ppm in thermal equilibrium to several percent after enhancement) within minutes to seconds.

In SEOP, a circularly polarized laser beam with a particular wavelength is used to irradiate a tiny amount of alkali metal vapor together with  $^{129}\text{Xe}$  gas in the presence of an appropriate magnetic field. This gives rise to a high electron spin polarization of the alkali metal atom, which can then participate in spin-exchange collision with the non-polarized  $^{129}\text{Xe}$  gas. As a consequence, the angular momentum of the alkali metal atom will be transferred to a  $^{129}\text{Xe}$  nucleus and yield hyperpolarized  $^{129}\text{Xe}$  gas. Compared with the polarization at thermal equilibrium under equivalent temperature and magnetic field conditions, the NMR signal enhancement via hyperpolarization can be 3–5 orders of magnitude [71, 72].

The PHIP techniques utilize enriched parahydrogen gas (a singlet isomer of dihydrogen) as the polarization source. Parahydrogen is a pure spin state of hydrogen but is NMR-silent due to its nuclear spin quantum number  $I = 0$ . To harness this pure spin state for NMR signal enhancement, the symmetry of the singlet spin state must be broken to allow evolution to the triplet state, preferably while magnetically coupled to a molecule of interest. In the hydrogenation class of PHIP, parahydrogen molecules are chemically introduced pairwise into a target molecule via a hydrogenation reaction, thereby joining the magnetic coupling network of the target molecule [73–75]. As an alternative to hydrogenation, SABRE works via formation of a reversible complex involving parahydrogen, the target substrate, and a polarization transfer catalyst which facilitates magnetic cou-

pling between the parahydrogen and target substrate. This method allows continuous hyperpolarization when replenishing the sample with fresh parahydrogen [76–81].

Applying gas-based hyperpolarization methods in liquid-state NMR requires one to dissolve the hyperpolarized gas species into the liquids containing the target molecules, followed by efficient detection of the enhanced molecules. The following factors are considered as the main challenges in the process to be faced:

### Solubility of the Hyperpolarized Gases and their Precursor in Solution

The hyperpolarized gases ( $^{129}\text{Xe}$ , parahydrogen) discussed in this review are relatively hydrophobic, which is an obstacle in dissolving such gases in polar (bio-relevant) liquids [82]. Thus, various approaches have been applied to improve the uptake of gas in solutions. The most straightforward method is increasing the injected gas pressure or the temperature. Laili et al. [83] observed the signal gains of SABRE hyperpolarization with increased parahydrogen gas pressure from 2 bar to 4 bar, and 40 % improved response with the overall polarization level by raising the temperature from 289 K to 308 K. Lehmkuhl et al. [84] also reported the correlation of signal enhancement with higher parahydrogen pressure in SABRE experiments. In addition to optimizing the experimental conditions (pressure, temperature), increasing the gas-liquid interface can enhance the dissolution process and will be discussed in detail later.

### Delivery of Hyperpolarized Compounds to the Detection Field

The detection of magnetic resonance signals of the hyperpolarized compounds is usually carried out in an NMR spectrometer, where the magnetic field is typically stronger than 1 T. However, the optimal polarization transfer field in SABRE experiments is lower than this. For instance, the magnetic field strength of 6.5 mT is sufficient for spin order derived from parahydrogen spontaneously transferred to the  $^1\text{H}$  sites on co-ligand substrates [85], and micro-Tesla or even nano-Tesla to achieve efficient direct polarization of heteronuclei ( $^{13}\text{C}$ ,  $^{15}\text{N}$ ,  $^{31}\text{P}$ ) [86–88]. In the case of  $^{129}\text{Xe}$  hyperpolarization via SEOP, the optimal magnetic field is generally on the order of 10 mT. Therefore, the transport of hyperpolarized compounds into the detection field is the prerequisite for measuring the hyperpolarized signal with high quality spectroscopic resolution. In the case of PHIP, the delivery should be as fast as possible to eliminate polarization attenuation caused by relaxation. For  $^{129}\text{Xe}$ , where the hyperpolarized gas state has much slower relaxation, the delivery distance should be minimized to avoid spin relaxation due to the collision between  $^{129}\text{Xe}$  molecules and the pipe wall.

Experimentally, gas-based hyperpolarization in the liquid NMR state is typically achieved by bubbling the hyperpolarized gas species into the sample solution to achieve intense gas-liquid contacting at the macroscale. The most accessible

and simple technique is bubbling parahydrogen gas via a capillary insert into the NMR sample tube or using high-pressure NMR tubes to pressurize the parahydrogen gas and then manually shake the tube for efficient contacting. For SABRE experiments, a high-pressure NMR tube is pressurized with parahydrogen followed by shaking the tube in the stray field of the high-field NMR magnet (i.e., at the top of the superconducting magnet) before rapid transfer into the magnet for NMR acquisition [89]. This procedure has been used extensively in many studies of new substrates or catalytic systems of SABRE.

Cowley et al. [90] conducted SABRE experiments in an automated gas-liquid contacting system (polarizer) for SABRE, where the parahydrogen gas was bubbled through a glass frit located at the bottom of a mixing chamber contained the sample solution. A solenoid copper coil arranged to surround the mixing chamber delivered the optimal polarization transfer field. After a predetermined bubbling time period, the parahydrogen gas dissolved in the solution after which the hyperpolarized solution was conveyed to the NMR flow probe for signal acquisition via a liquid transfer line connected to the chamber. In this automated apparatus, the flow rate and the bubbling time was computer controlled and thus ensured a high level of reproducibility.

This automated polarizer (Fig. 4a) has been exploited for studying the impact of experimental variables, such as the bubbling time at which parahydrogen gas was introduced into the solution, the pressure of parahydrogen gas in the mixing chamber, and the magnetic field strength on efficiency of SABRE hyperpolarization [85]. Consequently, optimization of the SABRE method and maximization of signal enhancement was achieved.

Several years later, a modified version of the polarization system, compatible with benchtop NMR spectrometers, was applied to continuously re-polarize the sample solution [91]. In this work, the highly reproducible signal enhancement facilitated SABRE hyperpolarized multi-dimensional NMR benchtop spectroscopy. In addition, Hill-Casey et al. [92] explored a similar automated bubbling setup for in situ SABRE experiments in the Earth magnetic field, in which

the build-up process of observable SABRE hyperpolarized signal was a function of the total parahydrogen bubbling time (Fig. 4b)).

Although gas bubbling utilizing batch-type hyperpolarization offers its own merits for gas-liquid contacting, the bubbling method at the macroscale still faces the following limitation. Firstly, gas bubbles create havoc with magnetic field homogeneity because the gas' magnetic susceptibility differs from that of the surrounding liquid phase. Therefore, the spectral resolution deteriorates significantly. The stop flow strategy has been used to maintain spectral resolution at the cost of losing polarization, due to delay caused by switching off the flow [93] (Fig. 4c). Secondly, it suffers from an inherent gas-liquid mass transfer limitation due to low interfacial areas, which is determined by the surface area of the generated bubbles, resulting in prolonged experimental time (hindering gas-liquid-based reaction monitoring). Finally, handling flammable and hazardous hydrogen gas in batch hyperpolarization can harbor a severe safety issue.

Baumer et al. [94] first proposed dissolving hyperpolarized  $^{129}\text{Xe}$  in different solutions ( $\text{H}_2\text{O}$ , DMSO, and bioliquid containing phospholipid biocelles) by using a hollow fiber membrane contactor (Fig. 5a). The hollow fiber membrane acts like a micro sieve, in which the hydrophobicity prevents fluids from wetting the wall of the fibers. The gas diffused through the micropores distributed in the membrane and dissolved in the liquid phase inside the hollow fiber. Amor et al. [100] produced a contrast agent for clinical MRI application (lung phantom) via passing the hyperpolarized gas through a hollow membrane contactor (Fig. 5b). Later, the same group conducted quantitative MRI imaging studies of blood-dissolved hyperpolarized  $^{129}\text{Xe}$  in different membrane materials by exploiting a hollow fiber membrane module [95]. Cleveland et al. [101] achieved 3D MR imaging of a living animal's lung by enriching hyperpolarized  $^{129}\text{Xe}$  in rat blood. The hollow fiber-based membrane contactor has also been applied in Phip experiments at high-field (PASADENA) [95] (Fig. 5c). It has been demonstrated that utilizing the hollow fiber membrane contactors for dissolving hyperpolarized gas substances is fast, robust, and

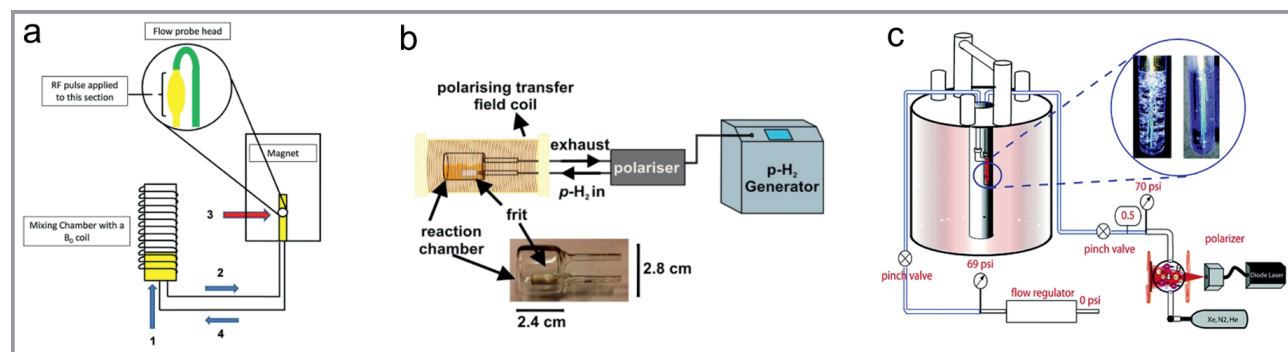


**Figure 4.** Overview of bubbling apparatus used in gas-based hyperpolarization technologies. a) Schematic of the automated polarizer for SABRE [85], (c) 2014, John Wiley & Sons. b) Schematic of an in situ SABRE hyperpolarization system in the Earth magnetic field, Hill-Casey et al. [92], © 2015, MDPI. c) Bubbling set-up with pneumatic valves for laser enhanced  $^{129}\text{Xe}$  polarization. The bubbling dispenser was located in the magnet [93], © 2006, American Chemical Society.

without the formation of foam or bubbles, thus diminishing the deleterious effects on NMR spectral resolution.

In addition to the hollow fiber contactor, a flat membrane configuration with has also been explored to accomplish gas-based hyperpolarization. Lehmkuhl et al. [84] utilized a flat membrane contactor for continuously high polarization of target molecules via the SABRE method using benchtop NMR systems. In addition, the influence of experimental conditions such as flow rate and pressure of both phases on signal enhancement was studied in detail. A membrane contactor with meandered microchannels was fabricated by 3D printing, and a composite membrane was used to separate the gas and liquid phase. During the experiments, the membrane contactor was located near the NMR spectrometer, and the polarized solution was transported to the detection area by a short length of tubing, to minimize loss of polarization via relaxation.

Bordonali et al. [97] designed and fabricated a micro-polarizer for in situ chemosensing SABRE processes at a high-field (11.7 T) (Fig. 5d). The micro-polarizer consisted of a micro gas-liquid contactor for introducing

parahydrogen gas into a sample solution. The gas and liquid microchannels with dimensions  $300\ \mu\text{m} \times 100\ \mu\text{m}$  ( $= \text{width} \times \text{depth}$ ) were engraved on two  $210\ \mu\text{m}$  thick glass substrates respectively by nanosecond laser cutting. A  $20\ \mu\text{m}$  thick PDMS membrane fabricated by spin coating was plasma bonded between the channel faces of the two glass layers. The parahydrogen gas diffused across the membrane and then dissolved in the liquid phase. The SABRE experiments were performed at high-field using a custom Helmholtz microcoil, and the NMR hydride signals of hydrogen bound to the catalyst, appearing in the spectral region from  $-22\ \text{ppm}$  to  $-23\ \text{ppm}$ , were explored as a probe for SABRE-based chemosensing with picomole sensitivity.

Eills et al. [98] conducted PHIP experiments on a micro gas-liquid contactor compatible with a custom transmission line probe. Thin PMMA sheets with cut channel structures were directly bonded together with a solvent plasticizer (Fig. 5e). Unlike the sandwich layout of the flat membrane contactor mentioned before, the silicon elastomer PDMS membrane attached at the liquid channel side acted as both

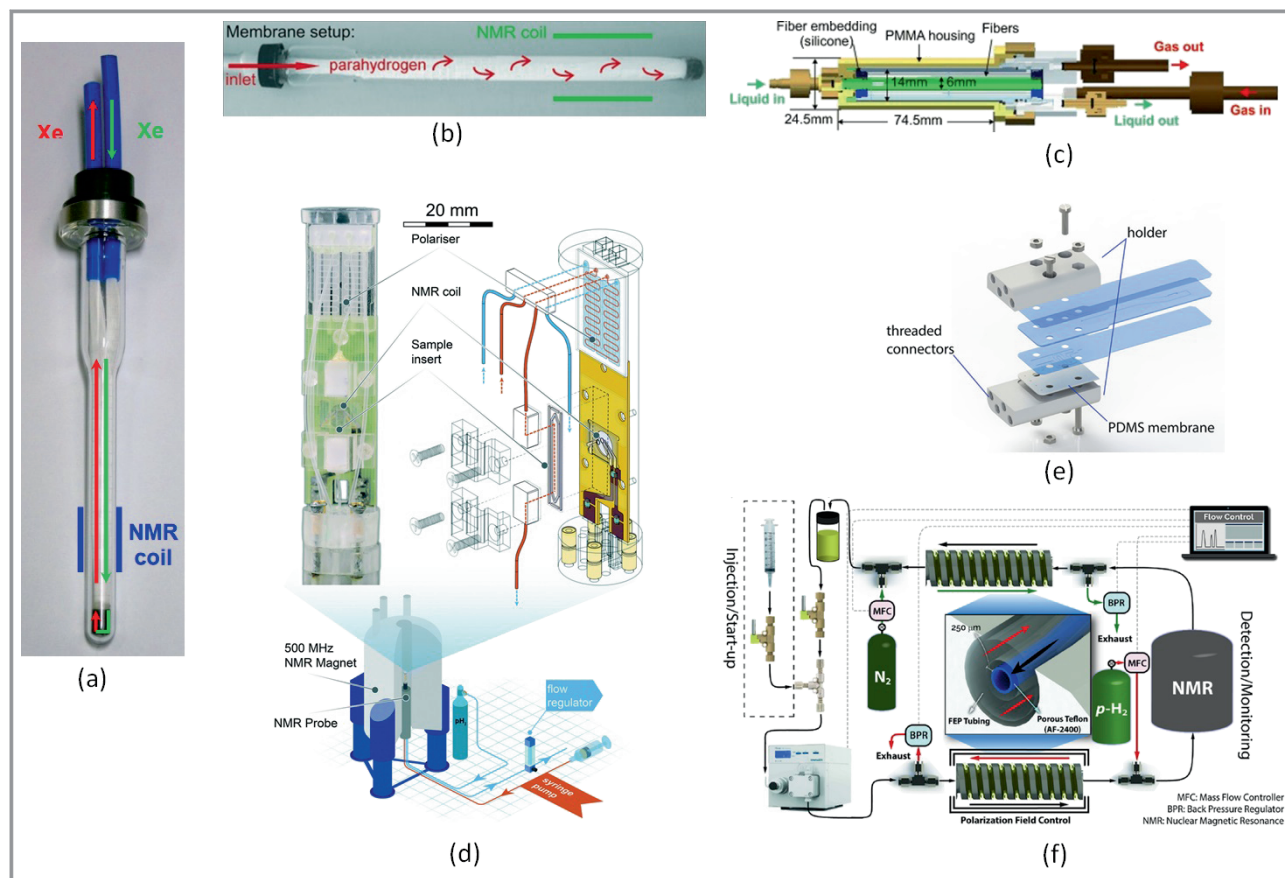


**Figure 5.** Overview of micro gas-liquid contactors in gas-based hyperpolarization technologies. a) Membrane device for dissolving the  $^{129}\text{Xe}$  gas in a 10 mm NMR tube [94], © 2006, Wiley-VCH. b) Schematic of a hollow fiber membrane in a xenonizer setup [95], © 2011, Wiley-VCH. c) The hollow fiber membrane implemented in PHIP [96], © 2010, Wiley-VCH. d) The micro-SABRE platform consisted of a membrane gas-liquid contactor, a microfluidic chip and a micro-Helmholtz coil for chemosensing [97], © 2019, The Royal Society of Chemistry. e) Schematic of a gas-liquid contactor for PHIP. The chip device is a three layers configuration of PMMA-PMMA-PDMS [98], © 2019, American Chemical Society. f) A flow reactor system consisted of two tube-in-tube contactors, tee unions, mass flow controller and pumps for producing continuous hyperpolarization on substrates by SABRE [99], © 2021, Wiley-VCH.

diffusion media and fluid sealing. Parahydrogen gas flowing in the gas channel diffused throughout the bulk PDMS membrane and contacted the solution in the liquid channel above the membrane. The performance of PHIP hyperpolarization could achieve high resolution with picomole sensitivity.

More recently, TomHon et al. [99] utilized a gas-liquid reactor system with a tube-in-tube configuration to yield continuous  $^1\text{H}$ ,  $^{13}\text{C}$  and  $^{15}\text{N}$  hyperpolarization on various substrates by SABRE (Fig. 5f). The highly gas-permeable AF 2400 tubing inserted in an outer FEP tubing significantly increased the mass transfer rate of parahydrogen. The two tube-in-tube gas-liquid contactors were arranged both upstream and downstream to efficiently deliver and subsequently remove the hydrogen gas. In the secondary tube-in-tube contactor, inert gas with lower pressure with respect to the liquid phase was delivered in the outer tubing to reduce the concentration of the remaining parahydrogen gas in the solution flowing in the inner AF 2400 tube. The degassing process enabled a better saturation of the fresh parahydrogen gas in the primary contractor, and thus optimized the polarization level. With the higher polarization level provided with the tube-in-tube reactor, Yang et al. conducted continuous PHIP pumped RASER (Radio-frequency Amplification by Stimulated Emission of Radiation) to study the non-linear effects. [102]

### 3.2 Chemical Process Engineering

As outlined by Kockmann [103], process engineering encompasses fluid dynamics, multi-phase flow, transport processes, and chemical reactions, applied to chemical plants, power generation, food technology, and pharmaceuticals. The key unit operations in process engineering are mixers, heat exchangers, separators, and reactors. In recent years, there has been a trend towards miniaturization of these critical components. This has led to a so-called process intensification [104], leading in several phenomena such as increased heat and mass transfer rates, improvement of yield and selectivity in reactions, and consequently, has resulted in an improvement of production efficiency. Furthermore, it has made possible more precise control of chemical processes and has improved safety for dangerous reactions (reactants and/or products, and in managing harsh conditions such as high temperature and pressure.

Mixers are amongst the main operation units in process engineering and have been studied extensively [105, 106]. These devices can be classified according to their working principle, namely active and passive (or static) mixers. Due to ease of manufacturing, passive mixers are more widely used, especially when integrating them in NMR setups. Micro heat exchangers possess an increased surface-to-volume ratio and higher heat transfer rates in comparison to macro heat exchangers, which also leads to more precise thermal process control [107]. A crucial aspect is the

material selection, given the need of high temperature resistant materials, which leads to most micro heat exchangers being made out of metals, and hence are not NMR-compatible. In this sense, the previously mentioned developments in 3D printing of ceramics and glass play an important role.

In its widest definition, a reactor is a device in which a chemical, biochemical, or biological reaction takes place. Depending on the analyzed process, the reactor can integrate additional operation units, such as mixers for the introduction of reactants, or heat exchangers for regulating the process temperature. Reactors can be operated in batch, semi-batch, or continuous (plug flow) mode. The miniaturization of reactors has led to increased transfer rates for mass and heat, and to increased surface-to-volume ratios. Micro reactors do not only offer the benefit of process intensification and increased parameter control, but also safety, and thus, novel operating windows [62]. The integration of micro reactors with several spectroscopic methods, including NMR, have been reviewed by Yue et al. [108], covering the period until 2012, and more recently, by Rizkin et al. [109], up to 2019.

In the area of industrial process engineering, operation units can feature dimensions up to the order of many meters, whereas for micro devices, typical inner dimensions are in the micrometer range. In this section, devices with dimensions in both the micrometer and millimeter range, and which have been implemented within an NMR setup, will be considered. The applications are classified in two categories: the use of NMR to characterize the device, and the use of NMR to analyze the chemical process taking place within the system.

#### NMR for Device Characterization

Significant achievements have been made in the last 10 years to characterize passive mixers, with magnetic resonance imaging (MRI) showing its capacity for characterizing the velocity field within mixers. In comparison to other methods, MRI has the advantage of being non-destructive, being able to characterize the flow within opaque materials, and not needing tracers or inserts that might change the properties of the flow. In this regard, Tozzi et al. [110] studied the multi-lamination of the non-Newtonian shear thinning polymer called Carbopol, in a split and recombine (SAR) mixer within a 1 T permanent magnetic field with a spatial resolution of 0.5 mm. By doping one of the polymer inflows with manganese (II)-chloride ( $\text{MnCl}_2$ ) and performing a calibration of the signal intensity for different known concentrations, the authors were able to perform a quantitative study of the mixing within the first stages of the mixer. Insight was gained regarding the lamination behavior, which doubled only in the first three mixing stages, followed by an increase at a slower rate, which is in disagreement with the expected behavior. The authors asserted that such a study could be used to validate computational models of convection and diffusion in non-Newtonian fluids.

Similarly, Lim et al. [114] analyzed the laminar mixing of both Newtonian and non-Newtonian fluids in an SMX mixer ( $D_O = 25.4$  mm), using gadolinium chloride and manganese chloride as contrast agents, respectively, in a 1 T permanent magnet with a spatial resolution of 0.31 mm. The authors found that, for the Newtonian fluid and in the studied viscosity range, the viscosity had no significant influence on the mixing of the flow. However, the range that was explored was not extensive, and this affirmation might not always be true. Their experimental results also showed that the mixing of Newtonian fluids was better than that of non-Newtonian fluids. The authors pointed out that their experimental results seemed to be in disagreement with previous literature. Both of these studies have limitations, as at some point, the mixing occurs at such short length scales that it cannot be spatially resolved and suffer from significant volume effects. Mihailova et al. [111] complemented the previous setup by combining MRI with positron emission particle tracking (PEPT), analyzing the same Newtonian fluid as Lim et al. The data obtained using both methods was in good agreement, thus validating MRI as a method for flow characterization. An example of the mixing behavior in the first SMX element is shown in Fig. 6c.

Herold et al. [112] analyzed the flow velocity distributions within a static micro mixer using MRI velocimetry in a 200 MHz magnet with a spatial resolution of 0.19 mm. The goal was to observe the differences between two solutions,

one Newtonian and one non-Newtonian. A mixer was manufactured out of acrylic material using stereo lithography, and it was shown that it is possible to resolve the velocity components of both types of fluids. Furthermore, dead areas (low velocity) were revealed within the mixer. This insight is important when designing mixers for flowing polymers, as low velocities might lead to curing of the material and consequently clogging of the mixer. In Fig. 6b, a slice of the mixer for both the non-Newtonian and the Newtonian fluid is shown.

Motivated by the need of analyzing flow in opaque systems, Wiese et al. [115] studied a 3D-printed staggered herringbone micromixer (SHM) by means of 3D MRI velocimetry. The flow analysis is particularly challenging because of eddy flows induced by the geometry. The authors were able to map the velocity, with magnitudes up to  $22 \text{ mm s}^{-1}$  parallel, and  $4 \text{ mm s}^{-1}$  perpendicular to the flow direction. The experimental data was in good agreement with CFD simulations.

One of the main challenges of MRI is the achievable spatial resolution, which depends on several factors, such as detector (coil) and gradient, magnetic field strength and stability, and the fluid signal strength and temperature. Ahola et al. [113] achieved an in-plane resolution of  $39 \mu\text{m} \times 29 \mu\text{m}$  by using a tailored NMR surface coil, which enhanced the signal-to-noise ratio, and a pulsed-field-gradient spin-echo (PGSE) sequence. The velocity distribu-

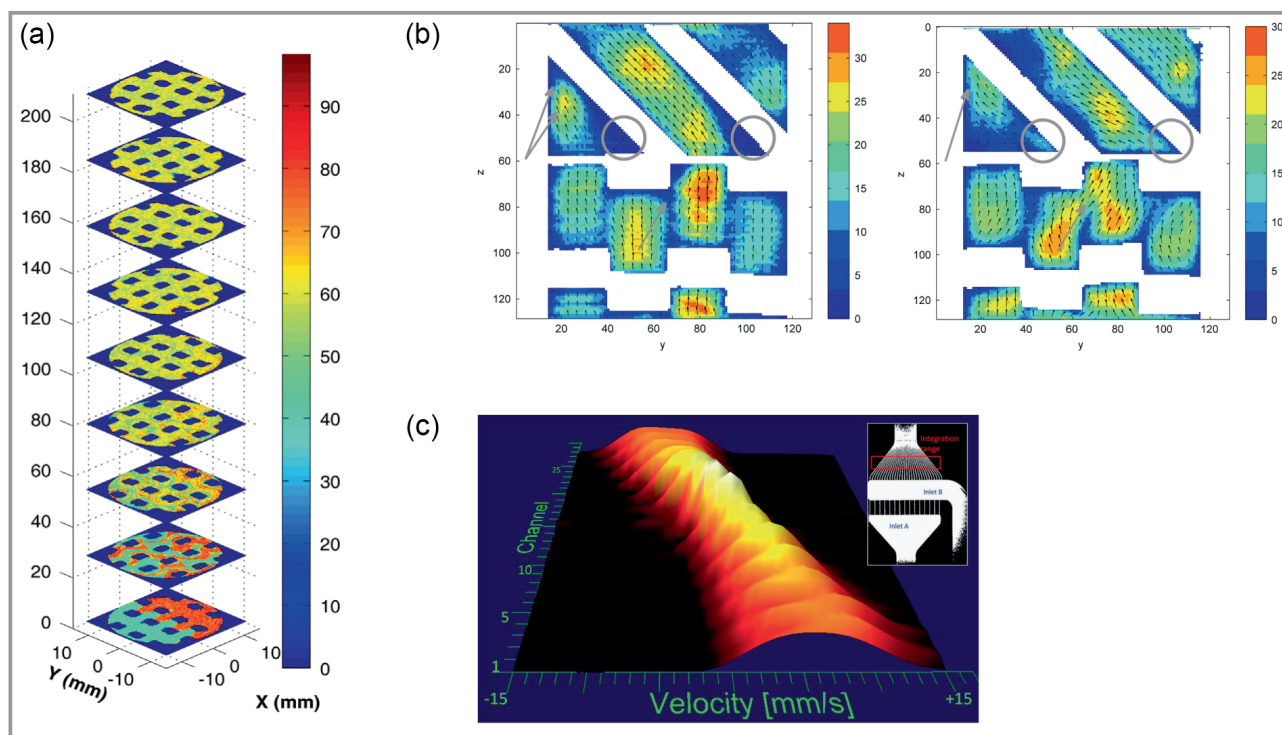


**Figure 6.** Magnetic resonance study of flow behavior in mixers. a) Mixing patterns of two glycerol streams at 50:50 volume ratio in the first SMX element [111], reprinted with permission from Elsevier. b) Magnitude of velocity and direction of flow in slice 12 of a setup for a xanthan solution  $0.4 \text{ mL s}^{-1}$  (left) and water  $2 \text{ mL s}^{-1}$  (right) [112], reprinted with permission from Elsevier. c) Propagators within channels in a selected region [113], Reproduced from Ahola et al. [113], with permission from the Royal Society of Chemistry.

tions in an interdigital glass micromixer with channel width and height of 65  $\mu\text{m}$  and 200  $\mu\text{m}$  were studied. The paper showed that the experimental velocity distributions obtained were in good agreement with theoretical predictions and could thus demonstrate that a 2D method circumvents the challenge of limited spatial resolution associated with 3D imaging methods. An example of the data obtained is shown in Fig. 6a.

### Chemical Process Analysis by Means of NMR

NMR is useful not only for characterizing a process within an operation unit, such as when analyzing the flow through a static mixer, but also for the in situ and/or operando monitoring of chemical reactions. The combination of NMR with miniaturized process engineering units opens up a new realm of possibilities in chemical analysis, and also allows for fresh insight. An example is the operando study of serial mixing experiments with volumes of less than 10  $\mu\text{L}$ , as performed by Plata et al. [116]. It was achieved in a microfluidic chip with pneumatic valves, creating a peristaltic flow within the chip when triggered sequentially as shown in Fig. 7. The mixing of sodium 3-trimethylsilyl-1-propane-sulfonate (DSS) and fumaric acid was performed by means of NMR spectroscopy. As noted, the setup could be improved and used to analyze more complex chemical reactions, however, always taking into account the NMR concentration limit of detection.

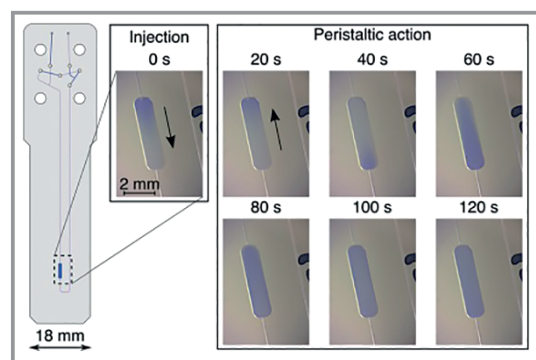


**Figure 7.** Peristaltic mixing mechanism in microfluidic chip from Plata et al. [116], where the arrows indicated the direction of the flow. Reproduced from Plata, M., Hale, W., Sharma, M., Werner, J. M., & Utz [116], M. Lab on a Chip. © 2021 with permission from the Royal Society of Chemistry.

An NMR flow cell with an integrated static micromixer was developed by Bornemann et al. [117]. The goal of this configuration was to minimize the time between the beginning of the chemical reaction and NMR data acquisition. Based on CFD simulations to optimize the micro mixer design, fabrication was accomplished by means of aluminum oxide additive manufacturing. The authors also took into consideration requirements for premagnetization of the flow, NMR spectral line shape, and residence time distribution. They achieved a robust system with a spectral quality comparable to standard NMR, which enabled quan-

titative studies of fast chemical reactions thanks to the minimized delay between mixing and acquisition.

Tijssen et al. [118] harnessed the benefits of miniaturization for in-line monitoring hydrogenation reactions of styrene, phenylacetylene, cyclohexene, and hex-5-en-2-one, with Pd catalyst particles. Their setup consisted of a tube-in-tube contactor for dissolving hydrogen gas in each of the solvents, a catalyst cartridge, and a fused silica capillary placed within a custom-made strip line detector. The hydrogen gas was dissolved in the liquid solvent in the tube-in-tube contactor at pressures of up to 7 bar. This circumvented some challenges of working with gases. The catalyst cartridge was placed within the magnet in order to assure complete magnetization of the sample and thus enable quantitative analysis. Embedding was possible due to the relatively small size of the cartridge, with outer diameter 1.59 mm and inner diameter 1.15 mm. The reaction volume in the setup was 208  $\mu\text{L}$ . The experiments were conducted at room temperature in a 14.1 T magnetic field. The authors gained insight in the solubility behavior of hydrogen in each of the solvents, noting that their observations when varying the flow rate did not align with the behavior expected from literature. Furthermore, they observed the optimal flow rate of each solvent for their respective hydrogenation reaction.

Ulpts et al. [119] studied the ethylene hydrogenation process within two different monolithic catalyst supports, a  $\gamma\text{-Al}_2\text{O}_3$  sponge, and a cordierite honeycomb, which were placed within a glass tube with inner diameter of 25 mm. Although the dimensions of this reactor are not in the micrometer range, it still demonstrates miniaturization in comparison to reactors found in industrial settings. The paper analyzed the reaction process by means of NMR spectroscopy along the length of the tube, in which the increase of the ethane signal was noticeably observed. It also analyzed the spatial distribution of the gas concentration by means of a 3D imaging pulse sequence. Furthermore, it compared the data acquired with NMR with that acquired with a mass spectrometer at the end of the reactor, as well as with a 1D model of the reactor, both comparisons were in good agreement. Not only reactions relevant to the chemical industry can be studied, but also from other interesting fields. Sesti et al. [120] implemented a cylindrical zirconia vessel with an inner diameter of 6.6 mm to study  $\text{CO}_2$  sequestration in minerals at elevated temperatures and pressures. The experimental setup implemented allowed to investigate the reaction with reactant flow-through at up to 150  $^\circ\text{C}$  and 140 bar.

Brächer et al. [121] developed a thermostatted micro reactor, which enabled monitoring of chemical reactions with fast kinetics. Their system integrated a micromixer with an NMR capillary flow cell, as shown in Fig. 8b. The first guarantees an efficient mixing of the reactants and, due to it being within the magnet, the time between mixing and signal acquisition was kept to a minimum. The reactants were kept at a constant temperature throughout their whole path. The capillary flow cell is made of silica glass, has a

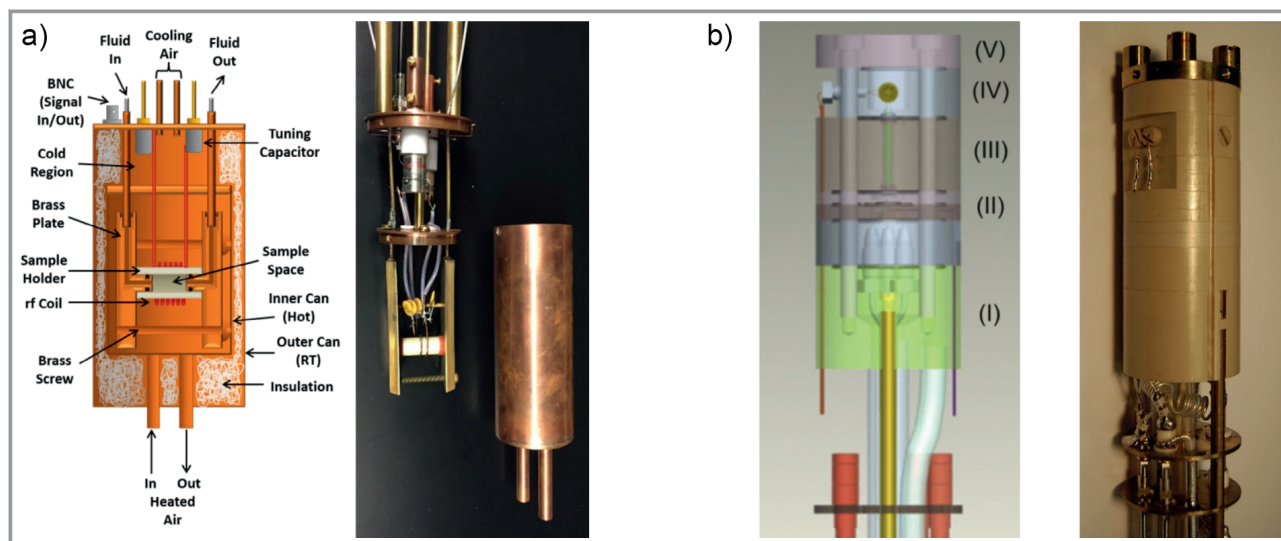


**Figure 8.** a) Schematic (left) and photo (right) of setup from Sesti et al. [120], reprinted with permission from Elsevier © 2017. b) Schematic (left) and photo (right) of the thermostatted micro reactor from Brächer et al. [121], reprinted with permission from Elsevier © 2014.

volume of 12  $\mu\text{L}$ , and is placed within a custom-made solenoidal micro detector. In a follow-up study [122], Brächer et al. analyzed two esterification reactions, one for formation of methyl acetate and the other for formation of methyl acetate, both homogeneously catalyzed with sulfuric acid. Temperatures were varied between 303 K and 333 K and the experiments were conducted in non-steady state stopped flow mode, achieving residence times of  $\sim 1.7$  s (time between mixing and acquisition). Measurements were performed in a 400 MHz NMR spectrometer. The fastest reaction studied was the esterification for methyl format formation with 6 wt % of sulfuric acid at 333 K, which reaches chemical equilibrium in less than 20 s, even in this case, enough data points were acquired, so that the course of reaction could be studied. The experimental results correlated well with kinetic models reported in literature, thus validating the usage of NMR and the developed micro reactor for the kinetic characterization of fast reactions.

Similar to Brächer et al. [121, 122], Hurtado Rivera et al. [123] developed a micro heat exchanger for controlling the temperature of a reaction occurring within an in situ reactor. A first prototype was produced by means of LCM. Here, a high aspect ratio cavity with inner microstructures for heat transfer enhancement was achieved. The device was located within the acquisition volume of the NMR magnet, which enabled operando monitoring of the reactions.

### 3.3 Metabolism Monitoring by NMR Using Microfluidic Platforms and Bioreactors

In this section, the focus turns to microfluidic platforms and bioreactors, specifically for cell culturing and metabolism monitoring combined with an application, and with NMR, with cell culturing being “the maintenance and

growth of cells in a controlled laboratory environment” [124]. As these platforms and bioreactors offer a plethora of possible applications (single cell analysis, organ- and body-on-chip, disease models, etc), there are many topics of importance but would go beyond the scope of the review. Qin et al. [125] wrote a comprehensive review for single-cell analysis in the context of drug screening, while a review of bioreactors with control of the gaseous environment as an example of environmental control and manipulation was published by Wu et al. [126]. The growing and promising field of organ-on-chip is thoroughly reviewed by Low et al. [127], discussing the challenges and advantages involved [128].

Nuclear magnetic resonance spectroscopy is a popular analysis tool for metabolic profiling as means to phenotype organisms and cell cultures. NMR spectroscopy enables detailed, non-invasive, non-destructive analysis of organism metabolism over extended periods. The metabolite levels and their fluctuations can be related to their metabolic pathways, yielding feedback on cell viability, aging processes, cell-cell interactions, and stress response. Additionally, the exo-metabolome, that is, metabolites excreted by an active biological system, also holds valuable information, as demonstrated by Palama et al. [129] who explored this aspect as a means to identify bacterial species.

For the observation of organism metabolism over time and in specific, controlled states (e.g., growth or stress), a cell culturing platform is beneficial. Bioreactors are defined as devices or containers “[...] in which a biological reaction or change takes place” [124]. Thus, they can contain enzymes, microorganisms, animal cells, plant cells, and tissues, and provide specific external environments for the biological system they contain [124]. Microfluidic bioreactors meet these criteria and operate on a micrometer scale. Hence, smaller amounts of samples are required. The

external cell environment inside the bioreactor is easier to control, as is similarly described for chemical reaction processes, resulting in conditions inside the bioreactors which are considerably more homogeneous than their large-scale counterparts [130, 131]. Moreover, it is easier to influence such homogeneous conditions, for example as in cases where concentration gradients may be desirable. A further advantage is the prospect of direct integration or coupling of cell analysis together with microfluidic bioreactors [132].

The following will focus on applications involving metabolic monitoring, profiling, and reaction monitoring in the context of bioreactor platforms and NMR analytics. Afterwards, the emphasis will turn to various options available to microfluidic bioreactors as an outlook to the possibilities NMR system integration, followed by a discussion of further possible combinations the NMR and microfluidic bioreactor field may hold.

### Metabolic Monitoring in NMR

Nuclear magnetic resonance spectroscopy is a non-invasive and quantitative analytical method with broad detection modalities especially interesting for examining biological samples. Currently, the established approaches for non-destructive tracking and monitoring cell metabolism can be divided into two classes. One option is to monitor the flow-through culture medium from a bioreactor. Another option is to implement a bioreactor within the NMR system to monitor the entire culture. This might be accomplished in the simplest case by using an NMR sample tube as a bioreactor, with various considerations for maintaining the correct culture environment and preventing cell sedimentation. In an alternative to the macroscopic approach, integra-

tion of a microfluidic platform or bioreactor into an NMR magnet is possible.

Maisch et al. [133] and Mehandale et al [134] used the first type, the analysis of the flow-through media from a bioreactor. For this, they fabricated a microfluidic bioreactor with hot embossing to examine the metabolic pathways of plant cells. The platform consisted of three layers, the top with a cell compartment and channels leading to and from the compartment, and a membrane layer for nutrition exchange with the bottom layer, implementing a transfer channel for nutrition supply and waste removal. The flow-through culture medium from the microfluidic bioreactor was collected and measured in time intervals, analyzed using NMR spectroscopy to establish and monitor the metabolic function of the plant cells over time [133].

Mehandale et al. [134] developed an NMR compatible platform, which offers the opportunity for real-time metabolic observation of biochemical processes. This was accomplished by placing a bioreactor outside of an 11.7 T NMR magnet and transporting culture medium from the bioprocess to the magnet over a tubing system using a peristaltic pump (Fig. 9). After  $^1\text{H}$  NMR detection, the collected sample was transported back into the bioreactor, with the entire sampling, measurement, and return process performed automatically. The monitoring of the process was demonstrated for 60 h of continuous measurement.

Xue et al. [135] coupled a bioreactor into an NMR system to monitor the metabolic pathways of the gram-positive, anaerobic, thermophilic, and acetogenic bacterium *Moorella thermoacetica*. This bacterium is potentially interesting for the industrial production of chemicals. The bioreactor consisted of a magnetic insert integrated with a bioreactor

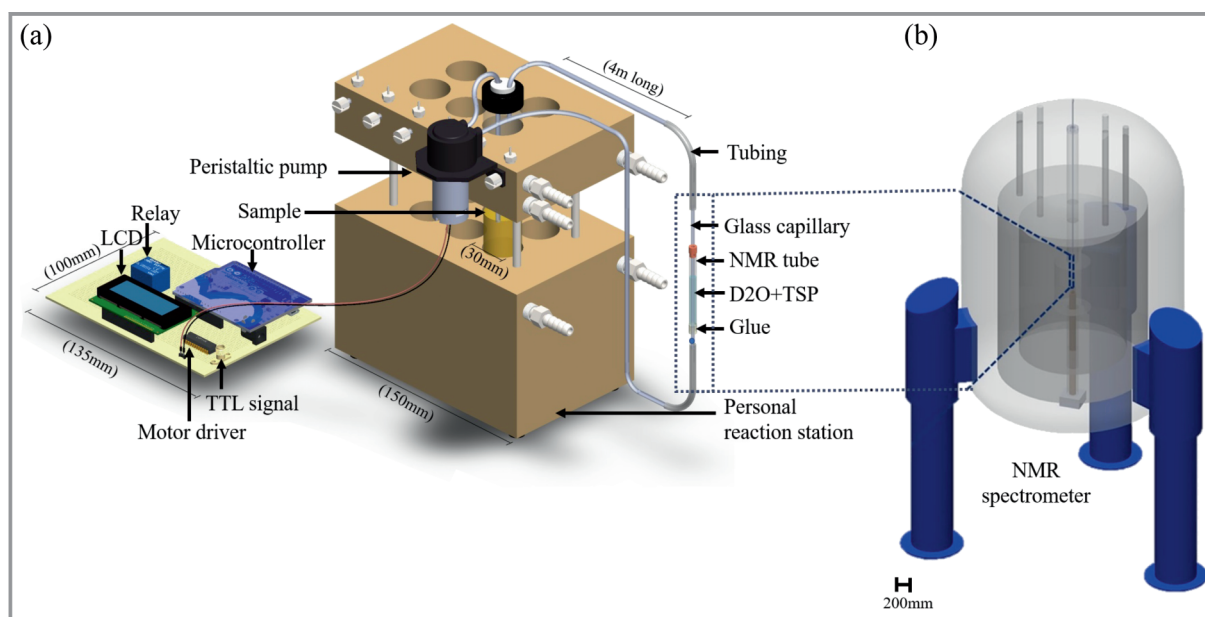


**Figure 9.** a) Setup of the control unit and bioreactor. b) Implementation of the setup in the NMR spectrometer. Adapted from Mehandale et al. [134]. © 2020 by the authors. Licensee MDPI, Basel, Switzerland.

controller, and a nonmagnetic cart, which supported culture media, vessels, gas, and electrical connections. The setup allowed precise control over the culture, monitoring cell growth with optical density measurements, and monitoring the sample over 48 h, with NMR measurements every 15 min. The setup allowed the characterization of bacterial growth.

The option of implementing a bioreactor in an NMR sample tube offers live monitoring of cells, and an NMR compatible platform for direct usage with most commercial NMR systems. Hertig et al. [136] converted a 5 mm NMR tube into a bioreactor to observe cellular metabolism and mitochondrial respiration. The cells were transported onto collagen-based membrane matrices, which was inserted into the NMR tube (Fig. 10). A flow tube unit connected to the bioreactor enabled temperature control, and gas mixing for a perfusion step. Alshamleh et al. [137] used NMR spectroscopy to monitor the metabolism of acute myeloid leukemia cells in real-time by storing the cell cultures in NMR tubes. They decided against an approach that prepares the cells in agarose, since this can negatively affect cell viability. Instead, the cells were prepared in a cell culture medium, with a cell-friendly matrix in an NMR tube to avoid sedimentation of the cells. The sample tubes were stored in a sample changer equipped with temperature control, and a robot that alternated the samples into the NMR without temperature change [137]. The experimental setup allowed the simultaneous monitoring of multiple samples over time. A similar approach was used by Wen et al. [138]. A comparison between the metabolism of healthy and cancerous cells was performed, and the effects of an anti-cancer drug on metabolism were observed successfully [138].

Beside the macro-bioreactor approach, the integration of microscale bioreactors directly within the NMR system has also been demonstrated. The microfluidic cell-culturing device from Yilmaz et al. [139] for perfusion of mammalian cells, as can be seen in Fig. 11 was designed to be directly inserted into the NMR magnet. Laser cutting and rastering was used to manufacture the microfluidic bioreactor. The device consists of three layers of PMMA, and a PDMS layer, which functions as a membrane for gas-liquid exchange. Using inlets and an outlet in the middle PMMA layer, nutrition was supplied, and waste could be transported out of the device. The device allowed in situ monitoring of cell metabolism while supplying sufficient oxygen for normoxic conditions for the cell culture. Patra et al. [140], likewise, employed laser cutting and rastering of PMMA sheets to manufacture a cell chip for culturing cancer cells and cell spheroids for time-resolved non-invasive monitoring by NMR. The device allowed cell culturing on the surface of the bottom channel, and single spheroid culturing by tilting the device during the culturing process. After culturing and spheroid formation, the cell chip was sealed and inserted into the NMR. Successful monitoring of the single cancer spheroid over time was demonstrated [140]. Montinaro et al. [141] developed microfluidic chips for sub-nL NMR spectroscopy with single-chip CMOS integrated detectors. The purpose of these chips was the analysis of single cells, mammalian egg cells, or living microscopic organisms through NMR spectroscopy. For this, the samples were trapped aligned to the micro-coil of the CMOS chip. Column geometries were used for narrowing the channel and impede further movement of cells. The chip was manufactured via two-photon polymerization 3D printing. For

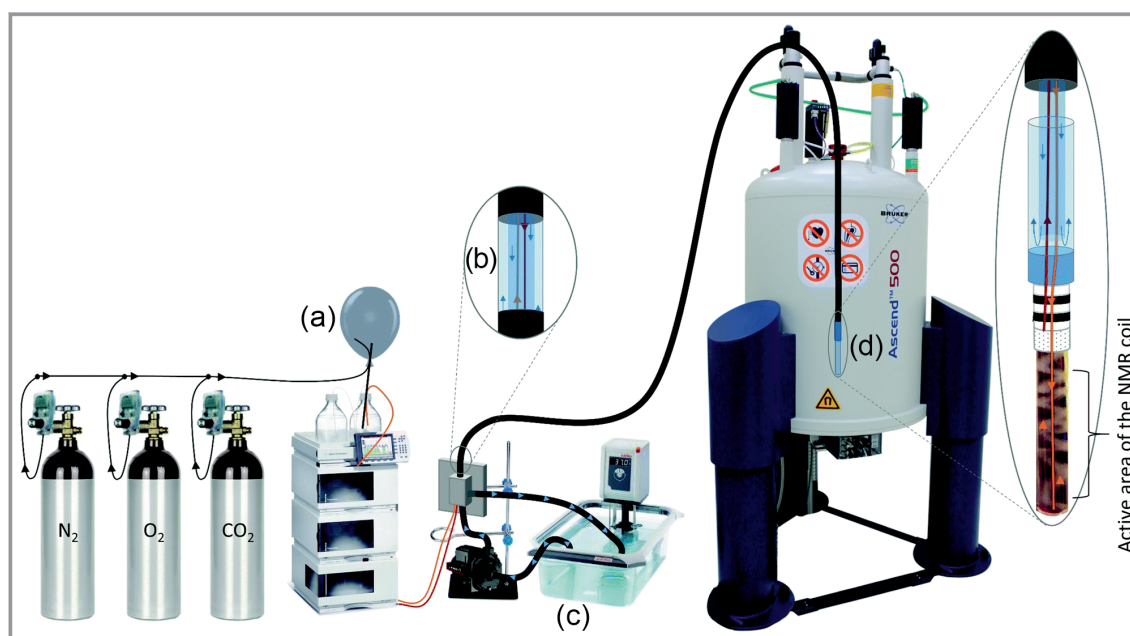


**Figure 10.** Setup of the NMR sample tube bioreactor by Hertig et al. [136] consisting of a) a gas blending system, b) a pumping system and c) a heated water bath. Reprinted with permission from the Royal Society of Chemistry © 2021.

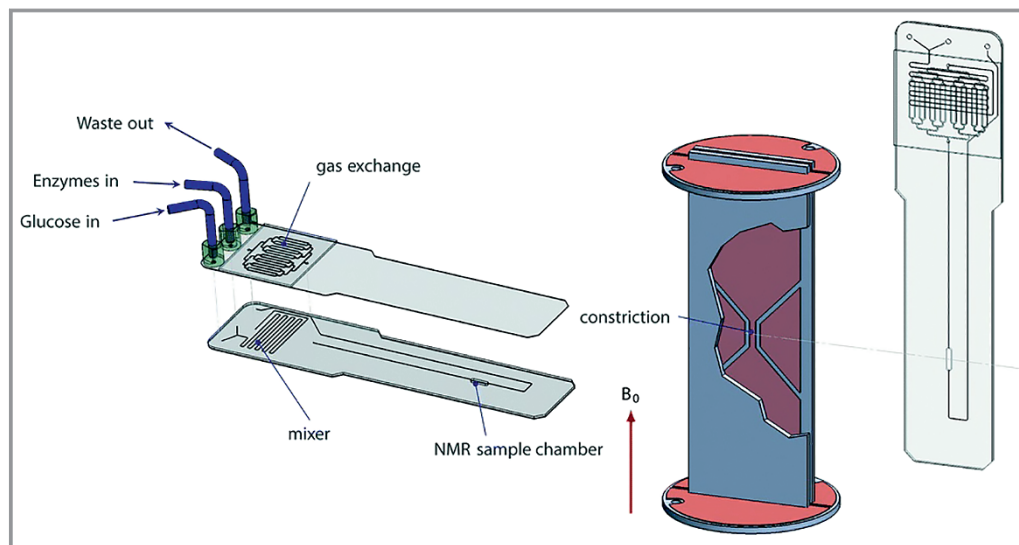


**Figure 11.** Perfusion culture chip by Yilmaz et al. [139] for characterization of oxygen permeation. Reproduced from Yilmaz et al. [139], *Lab Chip* 16 with permission from the Royal Society of Chemistry © 2016.

the structures an optically transparent IP-S photoresist was used. To create closed channels, a 500 nm thick water-soluble sacrifice layer was applied through spin coating, and after successful printing, were dissolved. With those two chip designs, Montinaro et al. [141] were able to conduct sub-nL NMR with a whole *Richtersius coronifer ovum*, and a subsection of a *Caenorhabditis elegans* in  $\text{H}_2\text{O}$  and  $\text{D}_2\text{O}$ . This approach tackled the previously mentioned drawbacks of low sensitivity, by implementing a microcoil detector, and experiment integration into the NMR setup by miniaturization of the hardware.

### Versatile Applications of Microfabrication for Bioreactors

While several examples of NMR compatible bioreactors have been demonstrated, there exists a large library of microfluidic bioreactors whose designed applications can benefit from insight gained by NMR spectroscopy. Kwak et al. [53] applied soft lithography molding to manufacture a microfluidic bioreactor which enables the high-throughput determination of the ideal growth and culture conditions of cell cultures. It was used to determine the optimal growth conditions of the microalgae *Neochloris oleoabundans* because of high potential as a potentially renewable resource for biomass and biofuel production, whilst consuming  $\text{CO}_2$  through photosynthesis. The materials of choice for the bioreactor, PDMS, and glass, are suitable for these organisms as they do not restrict the entry of light necessary for growth. The microfluidic bioreactor holds 16 chambers for parallel observation and detection of cell growth through optical density measurements, or fluorescence detection after cell treatment.

Ho et al. [54] manufactured a bioreactor to reproduce large-scale bioreactors by applying soft lithography molding. The PDMS based bioreactor consisted of supply

channels, channels for the control of nutrition supply, and growth chambers attached to the supply channels. The goal of this bioreactor was to reproduce the conditions found in large-scale bioreactors and estimate the influence of those conditions on cell growth. The experiment allowed detailed analysis of the culturing processes of large-scale bioreactors, determining issues and possible optimization potential for stable culturing processes.

Finkbeiner et al. [142] used hot embossing to manufacture a microfluidic bioreactor used to monitor plant cell-cell interactions. The top and bottom layers consisted of chambers separated through a membrane. The top part had holes for cell insertion into the chamber and was used for cell culturing, while the bottom layer had an inlet and an outlet into the chamber for culture media. The membrane between the layers allowed the interaction and nutrition exchange between cells in the top chamber with the medium in the chamber of the bottom part. The resulting metabolites were evaluated and analyzed [143]. The intention was to connect multiple of these reactors, each holding different cell types, to each other to transport the metabolites from one bioreactor to the next and allow specific cell-cell interaction between different cell types. This approach can be beneficial for finding an artificial pathway for producing plant metabolites, which are needed in different applications, e.g., the pharmaceutical industry, but were never produced in the laboratory before.

## 4 Conclusion and Outlook

NMR is an information-rich analytical method and has unfortunately been trapped behind large expertise and cost barriers preventing it from being fully exploited. One path towards improving the accessibility of the method is

through system miniaturization, where new types of experiments and experimental conditions can be explored that were, previously, difficult to achieve. In this review, the advantages and future trends of miniaturized systems applied to the sample handling and management of NMR-based chemical and biological process measurement were presented. Emphasis was placed on the basic criteria for selecting materials that satisfy both NMR- and application-specific constraints, together with the possibilities and limitations for the design and fabrication of such systems. Current standards and recent advances in microfabrication technologies, specifying their mechanism, possible resolutions, as well as advantages and disadvantages, were provided. Both the materials and manufacturing methods discussed were highlighted in the context of selected applications.

Manufacturing methods continue to evolve, achieving ever better feature resolutions, geometries with additional complexity, while accessing an ever-increasing variety of materials. As an example, the recently established two-photon polymerization technique, which enables dimensions in the nanometer range, has recently been used by Montinaro et al. to manufacture 3D-printed microchannels for sub-nL NMR spectroscopy.[141] Together with advances in manufacturing is the ability to tightly integrate additional functionalities, adding further experimental degrees of freedom. This work highlighted only three example applications, focusing on micro process engineering, which included the typical operation units (mixers, reactors and heat exchangers), fluidic setups for NMR-based metabolism monitoring, and gas-liquid micro contactors for gas-based hyperpolarization techniques.

There is a large number of microsystem and microfluidic options available in the literature, and only a small fraction has been explored in the context of NMR measurements. Certainly, NMR sensitivity plays a strong role in deciding whether a particular application and device will find a partner with NMR, however, hyperpolarization methods are beginning to bridge the sensitivity gap and have even started to enter into the micro-domain. As such gaps continue to close, numerous applications will stand to benefit, spanning process monitoring and technical reaction optimization under extreme (or industrially relevant) conditions, energy storage and transformation, to bio-systems and toxicity monitoring, drug screening, and metabolic monitoring in the context of disease models, including observation of culture growth, spheroid formation, and potentially single cell analysis. All of these examples have the potential to be supported by NMR-specific signal enhancement techniques, required when working with reduced sample volumes.

## Acknowledgements

J.G.K. acknowledges the support from an EU2020 FET grant (TiSuMR, 737043), ERC-SyG (HiSCORE, 951459), the framework of the German Excellence Initiative under DFG grant EXC 2082 “3D Matter Made to Order”, the DFG for funding the CRC 1527 “HyPERiON”, and the KIT-VirtMat initiative “Virtual Materials Design II”. J.J.B. acknowledges support from the DFG under grant number BR 4175/5-1. N.M. acknowledges support from the DFG under grant number MA 6653/3-1. J.J.B. and A.C.H.R. thank Dr. Karsten Seidel, Dr. Emma S. Thompson and Dr. Nikolaus Nestle for the fruitful discussions regarding NMR. All authors acknowledge the partial financial support of the Helmholtz Association through the program “Materials Systems Engineering — MSE”. The authors acknowledge the support of the Karlsruhe Nano Micro Facility (KNMFi), a Helmholtz Research Infrastructure at Karlsruhe Institute of Technology. Open access funding enabled and organized by Projekt DEAL.



**Julia Schulte-Hermann** obtained her Master of Science in mechanical engineering at the Karlsruhe Institute of Technology in Germany. Currently she is pursuing a PhD at the Institute of Microstructure Technology at the Karlsruhe Institute of Technology under Prof. Dr. Jan G. Korvink. Her work focuses on metabolism monitoring in NMR.



**Jing Yang** was born in 1991 in Shandong, China. She obtained a Master of Science in Mechatronics and Information Technology in 2020. Afterwards, she pursued a PhD program at the Institute of Microstructure Technology. Her work is focused on the development of microfluidic platforms for parahydrogen-based hyperpolarization.



**Andrea C. Hurtado Rivera** is a PhD candidate at the Institute of Microstructure Technology at the Karlsruhe Institute of Technology. She studied mechanical engineering at the Karlsruhe Institute of Technology, obtaining her Bachelor of Science in 2018 and Master of Science in 2019. Her research focuses on the development of 3D-printed

ceramic reactors for operando NMR measurements under harsh conditions, such as elevated temperature and pressures.



**Prof. Dr. Jan G. Korvink** directs the Institute of Microstructure Technology at the Karlsruhe Institute of Technology. His 30-person-strong research group is active in the field of MEMS technology and applications, with a focus on nuclear magnetic resonance (NMR). He is currently funded by the European Research Council through

the Synergy Grant HiSCORE, addressing drug screening via NMR, and through the German Research Foundation (DFG) via a Collaborative Research Centre, CRC 1527 HyPERiON, on the topic of compact NMR hardware. His research has been reported in more than 280 journal articles.



**Neil MacKinnon** obtained his BSc in chemistry from the University of Toronto in 2004. He continued at the University of Toronto and obtained his PhD in 2009 with Prof. P. Macdonald. He then moved to the University of Michigan and performed his post-doctoral work with Prof. A. Ramamoorthy, before joining the group of Prof. J. Korvink at

the University of Freiburg as a group leader in 2013. In 2015 the group moved to the Karlsruhe Institute of Technology where he continues as a group leader. His research revolves around developing and using NMR methods to investigate small, active systems. With the improved methods and hardware, the aim is to obtain molecular profiles of large sample numbers with measurement time resolution on the order of seconds.



**Juergen J. Brandner** studied Chemistry at the University Heidelberg and Electrical Engineering at Technical University Karlsruhe, where he obtained his PhD in Mechanical Engineering. He got his Habilitation in Chemical Process Engineering at Technical University Dresden. He is Professor (hon) for Micro Process Engineering at

Technical University Dresden, and lecturer at Karlsruhe Institute of Technology. Many years he worked in the topic of Thermal and Chemical Micro Process Engineering. In 2017 he joined the Korvink Group at Institute of Microstructure Technology (IMT). He additionally became Scientific Director of the Karlsruhe Nano Micro Facility KNMFi ([www.knmf.kit.edu](http://www.knmf.kit.edu)).

## References

- [1] B. Blümich, P. Blümich, Pauly, *Essential NMR*, Springer, Heidelberg 2005.
- [2] A. G. Webb, *NMR Spectrosc. Pharm. Anal.* **2008**, 83–130.
- [3] C. J. Jones, C. K. Larive, *Anal. Bioanal. Chem.* **2012**, *402*, 61–68.
- [4] S. S. Zalesskiy, E. Danieli, B. Blumich, V. P. Ananikov, *Chem. Rev.* **2014**, *114* (11), 5641–5694.
- [5] C. Massin, F. Vincent, A. Homsy, K. Ehrmann, G. Boero, P.-A. Besse, A. Daridon, E. Verpoorte, N. F. De Rooij, R. S. Popovic, *J. Magn. Reson.* **2003**, *164* (2), 242–255.

- [6] A. Dupré, K.-M. Lei, P.-I. Mak, R. P. Martins, W. K. Peng, *Microelectron. Eng.* **2019**, *209*, 66–74.
- [7] W. Liu, Y. Zhu, *Anal. Chim. Acta.* **2020**, *1113*, 66–84.
- [8] J. G. Korvink, N. MacKinnon, V. Badilita, M. Jouda, *J. Magn. Reson.* **2019**, *306*, 112–117.
- [9] J. B. Erhardt, E. Fuhrer, O. G. Gruschke, J. Leupold, M. C. Wapler, J. Hennig, T. Stieglitz, J. G. Korvink, *J. Neural Eng.* **2018**, *15* (4), 041002. DOI: <https://doi.org/10.1088/1741-2552/aab4e4>
- [10] F. Cardarelli, *Mater. Des.* **2001**, *22* (3), 237. DOI: [https://doi.org/10.1016/s0261-3069\(00\)00075-3](https://doi.org/10.1016/s0261-3069(00)00075-3)
- [11] M. Getzlaff, *Fundamentals of Magnetism*, Springer Science & Business Media, Heidelberg **2007**.
- [12] E. Fuhrer, M. Jouda, C. O. Klein, M. Wilhelm, J. G. Korvink, *IEEE Trans. Biomed. Eng.* **2020**, *67* (3), 915–923. DOI: <https://doi.org/10.1109/TBME.2019.2923693>
- [13] F. Jia, R. Kumar, J. G. Korvink, *Magn. Reson. Med.* **2013**, *69* (4), 1146–1156.
- [14] J. F. Schenck, *Med. Phys.* **1996**, *23* (6), 815–850. DOI: <https://doi.org/10.1118/1.597854>
- [15] M. C. Wapler, J. Leupold, I. Dragonu, D. von Elverfeld, M. Zaitsev, U. Wallrabe, *J. Magn. Reson.* **2014**, *242*, 233–242. DOI: <https://doi.org/10.1016/j.jmr.2014.02.005>
- [16] [www.schott.com/en-us/products/duran-p1000368/technical-details](http://www.schott.com/en-us/products/duran-p1000368/technical-details)
- [17] T. R. Dietrich, A. Freitag, R. Scholz, *Chem. Eng. Technol.* **2005**, *28* (4), 477–483.
- [18] T. Frank, *Microreactors Org. Chem. Catal.* **2013**, 53–80.
- [19] J. M. Bolivar, M. A. Tribulato, Z. Petrasek, B. Nidetzky, *Biotechnol. Bioeng.* **2016**, *113* (11), 2342–2349.
- [20] M. Takeda, K. Hallenga, M. Shigezane, M. Waelchli, F. Löhr, J. L. Markley, M. Kainosho, *J. Magn. Reson.* **2011**, *209* (2), 167–173.
- [21] F. Cardarelli, *Materials Handbook A Concise Desktop Reference*, Springer, London **2008**, 593–689.
- [22] B. Jiang, T. Maeder, A. J. Santis-Alvarez, D. Poulidakos, P. Mural, *J. Power Sources.* **2015**, *273*, 1202–1217.
- [23] B. Alm, R. Knitter, J. Hausselt, *Chem. Eng. Technol.* **2005**, *28* (12), 1554–1560.
- [24] P. Bemnowicz, M. Malodobra, W. Kubicki, P. Szczepańska, A. Górecka-Drzazga, J. Dziuban, A. Jonkisz, A. Karpiewska, T. Dobosz, L. Golonka, *Sens. Actuators, B* **2010**, *150* (2), 715–721.
- [25] M. B. Erlach, C. E. Munte, W. Kremer, R. Hartl, D. Rochelt, D. Niesner, H. R. Kalbitzer, *J. Magn. Reson.* **2010**, *204* (2), 196–199.
- [26] M. R. Arnold, H. R. Kalbitzer, W. Kremer, *J. Magn. Reson.* **2003**, *161* (2), 127–131.
- [27] D. Parker, J. Bussink, H. T. van de Grampel, G. W. Wheatley, E. Dorf, E. Ostlinning, K. Reinking, F. Schubert, O. Jünger, in *Ullmann's Encyclopedia of Industrial Chemistry*, Wiley-VCH, Weinheim **2000**.
- [28] H. M. Hegab, A. ElMekawy, T. Stakenborg, *Biomicrofluidics* **2013**, *7* (2), 21502.
- [29] C. Schmidleithner, D. M. Kalaskar, in *Stereolithography*, IntechOpen **2018**.
- [30] S. Waheed, J. M. Cabot, N. P. Macdonald, T. Lewis, R. M. Guijt, B. Paull, M. C. Breadmore, *Lab Chip* **2016**, *16* (11), 1993–2013.
- [31] J. Stampfl, S. Baudis, C. Heller, R. Liska, A. Neumeister, R. Kling, A. Ostendorf, M. Spitzbart, *J. Micromech. Microeng.* **2008**, *18* (12), 125014.
- [32] F. Kotz, K. Arnold, W. Bauer, D. Schild, N. Keller, K. Sachsenheimer, T. M. Nargang, C. Richter, D. Helmer, B. E. Rapp, *Nature* **2017**, *544* (7650), 337–339.
- [33] M. Schwentenwein, P. Schneider, J. Homa, *Adv. Sci. Technol.* **2014**, *88*, 60–64. DOI: <https://doi.org/10.4028/www.scientific.net/AST.88.60>
- [34] M. Schwentenwein, J. Homa, *Int. J. Appl. Ceram. Technol.* **2015**, *12* (1), 1–7.
- [35] [www.lithoz.com/en/our-products/3D-printers](http://www.lithoz.com/en/our-products/3D-printers)
- [36] [https://lithoz.com/wp-content/uploads/2022/08/LITHOZ\\_Material\\_Folder\\_EN.pdf](https://lithoz.com/wp-content/uploads/2022/08/LITHOZ_Material_Folder_EN.pdf)
- [37] U. Scheithauer, E. Schwarzer, G. Ganzer, A. Kornig, W. Becker, E. Reichelt, M. Jahn, A. Hartel, H. J. Richter, T. Moritz, *Addit. Manuf. Strateg. Technol. Adv. Ceram. Ceram. Trans.* **2016**, *258*, 31–41.
- [38] U. Scheithauer, E. Schwarzer, T. Moritz, A. Michaelis, *J. Mater. Eng. Perform.* **2018**, *27* (1), 14–20. DOI: <https://doi.org/10.1007/s11665-017-2843-z>
- [39] J. de Jong, *Application of Membrane Technology in Microfluidic Devices*, Ph.D. Thesis, University of Twente **2008**.
- [40] A. Selimis, V. Mironov, M. Farsari, *Microelectron. Eng.* **2015**, *132*, 83–89.
- [41] *The new Quantum X shape for high-precision 3D Microfabrication*, Nanoscribe, **2021**. [www.nanoscribe.com/en/products/quantum-x-shape](http://www.nanoscribe.com/en/products/quantum-x-shape)
- [42] F. Kotz, A. S. Quick, P. Risch, T. Martin, T. Hoose, M. Thiel, D. Helmer, B. E. Rapp, *Adv. Mater.* **2021**, *33* (9), 2006341. DOI: <https://doi.org/10.1002/adma.202006341>
- [43] D. Schuocker, *Mater. Manuf. Process.* **1989**, *4* (3), 311–330.
- [44] M. I. Mohammed, M. N. H. Z. Alam, A. Kouzani, I. Gibson, *J. Micromech. Microeng.* **2016**, *27* (1), 15021.
- [45] M. Benton, M. R. Hossan, P. R. Konari, S. Gamagedara, *Micro-machines* **2019**, *10* (2). DOI: <https://doi.org/10.3390/mi10020123>
- [46] M. J. Madou, *Fundamentals of Microfabrication: The Science of Miniaturization*, CRC Press, Boca Raton, FL **2002**.
- [47] W. Menz, O. Paul, *Mikrosystemtechnik Für Ingenieure*, Wiley-VCH, Weinheim **2012**.
- [48] R. Tiron, L. Mollard, O. Louveau, E. Lajoinie, *J. Vac. Sci. Technol., B* **2007**, *25* (4), 1147–1151.
- [49] G. Grecni, E. Zanchetta, A. Pozzato, G. Della Giustina, G. Brusatin, M. Tormen, *Appl. Mater. Today* **2015**, *1* (1), 13–19.
- [50] Y. Xia, G. M. Whitesides, *Angew. Chem., Int. Ed.* **1998**, *37* (5), 550–575. DOI: [https://doi.org/10.1002/\(sici\)1521-3773\(19980316\)37:5<550::aid-anie550>3.0.co;2-g](https://doi.org/10.1002/(sici)1521-3773(19980316)37:5<550::aid-anie550>3.0.co;2-g)
- [51] L. C. DeBolt, J. E. Mark, *Macromolecules* **1987**, *20* (10), 2369–2374.
- [52] B. Patra, Y.-H. Chen, C.-C. Peng, S.-C. Lin, C.-H. Lee, Y.-C. Tung, *Biomicrofluidics* **2013**, *7* (5), 54114.
- [53] H. S. Kwak, J. Y. H. Kim, S. J. Sim, *Bioprocess Biosyst. Eng.* **2015**, *38*, 2035–2043.
- [54] P. Ho, C. Westerwalbesloh, E. Kaganovitch, A. Grünberger, P. Neubauer, D. Kohlheyer, E. von Lieres, *Microorganisms* **2019**, *7* (4), 105.
- [55] S. S. Deshmukh, A. Goswami, in *Mater. Today Proc.*, Vol. 26, Elsevier, Amsterdam **2019**.
- [56] L. Peng, Y. Deng, P. Yi, X. Lai, *J. Micromech. Microeng.* **2013**, *24* (1), 13001.
- [57] T. Glinsner, T. Veres, G. Kreindl, E. Roy, K. Morton, T. Wieser, C. Thanner, D. Treiblmayr, R. Miller, P. Lindner, *J. Vac. Sci. Technol., B* **2010**, *28* (1), 36–41.
- [58] M. Worgull, J.-F. Héту, K. K. Kabanemi, M. Hecke, *Microsyst. Technol.* **2008**, *14* (6), 767–773. DOI: <https://doi.org/10.1007/s00542-007-0492-0>
- [59] B. Y. Tay, L. Liu, N. H. Loh, S. B. Tor, Y. Murakoshi, R. Maeda, *Microsyst. Technol.* **2005**, *11*, 210–213.
- [60] V. Piotter, T. Hanemann, R. Ruprecht, J. Hausselt, *Microsyst. Technol.* **1997**, *3*, 129–133.

- [61] J. Giboz, T. Copponnex, P. Mélé, *J. Micromech. Microeng.* **2007**, *17* (6), R96.
- [62] A. Renken, M. N. Kashid, L. Kiwi-Minsker, *Microstructured Devices for Chemical Processing*, Wiley, Hoboken, NJ **2014**.
- [63] J. P. Mugler, T. A. Altes, *J. Magn. Reson. Imaging* **2013**, *37* (2), 313–331. DOI: <https://doi.org/10.1002/jmri.23844>
- [64] M. Salerno, T. A. Altes, J. P. Mugler, M. Nakatsu, H. Hatabu, E. E. de Lange, *Eur. J. Radiol.* **2001**, *40* (1), 33–44. DOI: [https://doi.org/10.1016/S0720-048X\(01\)00347-3](https://doi.org/10.1016/S0720-048X(01)00347-3)
- [65] Y. Ohno, H. Koyama, T. Yoshikawa, K. Matsumoto, M. Takahashi, M. Van Cauteren, K. Sugimura, *Am. J. Roentgenol.* **2011**, *197* (2), 279–285. DOI: <https://doi.org/10.2214/AJR.10.5350>
- [66] R. H. Acosta, P. Blümner, K. Münnemann, H.-W. Spiess, *Prog. Nucl. Magn. Reson. Spectrosc.* **2012**, *66*, 40–69. DOI: <https://doi.org/10.1016/j.pnmrs.2012.03.003>
- [67] J. Wolber, A. Cherubini, M. O. Leach, A. Bifone, *Magn. Reson. Med.* **2000**, *43* (4), 491–496. DOI: [https://doi.org/10.1002/\(SICI\)1522-2594\(200004\)43:4<491::AID-MRM1>3.0.CO;2-6](https://doi.org/10.1002/(SICI)1522-2594(200004)43:4<491::AID-MRM1>3.0.CO;2-6)
- [68] M. M. Spence, S. M. Rubin, I. E. Dimitrov, E. J. Ruiz, D. E. Wemmer, A. Pines, S. Q. Yao, F. Tian, P. G. Schultz, *Proc. Natl. Acad. Sci. U. S. A.* **2001**, *98* (19), 10654–10657. DOI: <https://doi.org/10.1073/pnas.191368398>
- [69] Y. Wang, I. J. Dmochowski, *Acc. Chem. Res.* **2016**, *49* (10), 2179–2187. DOI: <https://doi.org/10.1021/acs.accounts.6b00309>
- [70] E. Mari, P. Berthault, *Analyst* **2017**, *142* (18), 3298–3308. DOI: <https://doi.org/10.1039/c7an01088e>
- [71] H. Fujiwara, H. Imai, A. Kimura, *Anal. Sci.* **2019**, *35* (8), 869–873.
- [72] C. Witte, M. Kunth, J. Döpfert, F. Rossella, L. Schröder, *J. Visualized Exp.* **2012**, 67.
- [73] F. Reineri, E. Cavallari, C. Carrera, S. Aime, *Magn. Reson. Mater. Physics, Biol. Med.* **2021**, (0123456789). DOI: <https://doi.org/10.1007/s10334-020-00904-x>
- [74] R. A. Green, R. W. Adams, S. B. Duckett, R. E. Mewis, D. C. Williamson, G. G. R. Green, *Prog. Nucl. Magn. Reson. Spectrosc.* **2012**, *67*, 1–48. DOI: <https://doi.org/10.1016/j.pnmrs.2012.03.001>
- [75] W. Y. Wang, H. Hu, J. Xu, F. Deng, *Chin. J. Magn. Reson.* **2018**, *35* (3).
- [76] L. S. Lloyd, R. W. Adams, M. Bernstein, S. Coombes, S. B. Duckett, G. G. R. Green, R. J. Lewis, R. E. Mewis, C. J. Sleigh, *J. Am. Chem. Soc.* **2012**, *134* (31), 12904–12907. DOI: <https://doi.org/10.1021/ja3051052>
- [77] O. Semenova, P. M. Richardson, A. J. Parrott, A. Nordon, M. E. Halse, S. B. Duckett, *Anal. Chem.* **2019**, *91* (10), 6695–6701. DOI: <https://doi.org/10.1021/acs.analchem.9b00729>
- [78] S. B. Duckett, R. E. Mewis, *Acc. Chem. Res.* **2012**, *45* (8), 1247–1257.
- [79] P. J. Rayner, M. J. Burns, A. M. Olaru, P. Norcott, M. Fekete, G. G. R. Green, L. A. R. Highton, R. E. Mewis, S. B. Duckett, *Proc. Natl. Acad. Sci. U. S. A.* **2017**, *114* (16), E3188–E3194. DOI: <https://doi.org/10.1073/pnas.1620457114>
- [80] M. Grootveld, B. Percival, M. Gibson, Y. Osman, M. Edgar, M. Molinari, M. L. Mather, F. Casanova, P. B. Wilson, *Anal. Chim. Acta* **2019**, *1067*, 11–30. DOI: <https://doi.org/10.1016/j.jaca.2019.02.026>
- [81] J. R. Lindale, S. L. Eriksson, C. P. N. Tanner, Z. Zhou, J. F. P. Collett, G. Zhang, J. Bae, E. Y. Chekmenev, T. Theis, W. S. Warren, *Nat. Commun.* **2019**, *10* (1). DOI: <https://doi.org/10.1038/s41467-019-08298-8>
- [82] P. Berthault, C. Boutin, C. Martineau-Corcus, G. Carret, *Prog. Nucl. Magn. Reson. Spectrosc.* **2020**, *118–119*, 74–90. DOI: <https://doi.org/10.1016/j.pnmrs.2020.03.002>
- [83] W. Iali, P. J. Rayner, A. Alshehri, A. J. Holmes, A. J. Ruddlesden, S. B. Duckett, *Chem. Sci.* **2018**, *9* (15), 3677–3684.
- [84] S. Lehmkuhl, M. Wiese, L. Schubert, M. Held, M. Küppers, M. Wessling, B. Blümich, *J. Magn. Reson.* **2018**, *291*, 8–13. DOI: <https://doi.org/10.1016/j.jmr.2018.03.012>
- [85] R. E. Mewis, K. D. Atkinson, M. J. Cowley, S. B. Duckett, G. G. R. Green, R. A. Green, L. A. R. Highton, D. Kilgour, L. S. Lloyd, J. A. B. Lohman, *Magn. Reson. Chem.* **2014**, *52* (7), 358–369.
- [86] T. Theis, M. L. Truong, A. M. Coffey, R. V. Shchepin, K. W. Waddell, F. Shi, B. M. Goodson, W. S. Warren, E. Y. Chekmenev, *J. Am. Chem. Soc.* **2015**, *137* (4), 1404–1407.
- [87] V. V. Zhivonitko, I. V. Skovpin, I. V. Koptuyug, *Chem. Commun.* **2015**, *51* (13), 2506–2509.
- [88] M. E. Gemeinhardt, M. N. Limbach, T. R. Gebhardt, C. W. Eriksson, S. L. Eriksson, J. R. Lindale, E. A. Goodson, W. S. Warren, E. Y. Chekmenev, B. M. Goodson, *Angew. Chem., Int. Ed.* **2020**, *59* (1), 418–423.
- [89] L. Buljubasich, M. B. Franzoni, H. W. Spiess, K. Münnemann, *J. Magn. Reson.* **2012**, *219*, 33–40.
- [90] M. J. Cowley, R. W. Adams, K. D. Atkinson, M. C. R. Cockett, S. B. Duckett, G. G. R. Green, J. A. B. Lohman, R. Kerssebaum, D. Kilgour, R. E. Mewis, *J. Am. Chem. Soc.* **2011**, *133* (16), 6134–6137. DOI: <https://doi.org/10.1021/ja200299u>
- [91] P. M. Richardson, A. J. Parrott, O. Semenova, A. Nordon, S. B. Duckett, M. E. Halse, *Analyst* **2018**, *143* (14), 3442–3450. DOI: <https://doi.org/10.1039/c8an00596f>
- [92] F. Hill-Casey, A. Sakho, A. Mohammed, M. Rossetto, F. Ahwal, S. B. Duckett, R. O. John, P. M. Richardson, R. Virgo, M. E. Halse, *Molecules* **2019**, *24* (22), 1–16. DOI: <https://doi.org/10.3390/molecules24224126>
- [93] S.-I. Han, S. Garcia, T. J. Lowery, E. J. Ruiz, J. A. Seeley, L. Chavez, D. S. King, D. E. Wemmer, A. Pines, *Anal. Chem.* **2005**, *77* (13), 4008–4012.
- [94] D. Baumer, E. Brunner, P. Blümner, P. P. Zänker, H. W. Spiess, *Angew. Chem., Int. Ed.* **2006**, *45* (43), 7282–7284. DOI: <https://doi.org/10.1002/anie.200601008>
- [95] N. Amor, K. Hamilton, M. Küppers, U. Steinseifer, S. Appelt, B. Blümich, T. Schmitz-Rode, *ChemPhysChem* **2011**, *12* (16), 2941–2947. DOI: <https://doi.org/10.1002/cphc.201100446>
- [96] M. Roth, P. Kindervater, H. P. Raich, J. Bargon, H. W. Spiess, K. Münnemann, *Angew. Chem., Int. Ed.* **2010**, *49* (45), 8358–8362. DOI: <https://doi.org/10.1002/anie.201002725>
- [97] L. Bordonali, N. Nordin, E. Fuhrer, N. Mackinnon, J. G. Korvink, *Lab Chip* **2019**, *19* (3), 503–512. DOI: <https://doi.org/10.1039/c8lc01259h>
- [98] J. Eills, W. Hale, M. Sharma, M. Rossetto, M. H. Levitt, M. Utz, *J. Am. Chem. Soc.* **2019**, *141* (25), 9955–9963. DOI: <https://doi.org/10.1021/jacs.9b03507>
- [99] P. TomHon, S. Han, S. Lehmkuhl, S. Appelt, E. Y. Chekmenev, M. Abolhasani, T. Theis, *ChemPhysChem* **2021**. DOI: <https://doi.org/10.1002/cphc.202100667>
- [100] N. Amor, P. P. Zänker, P. Blümner, F. M. Meise, L. M. Schreiber, A. Scholz, J. Schmiedeskamp, H. W. Spiess, K. Münnemann, *J. Magn. Reson.* **2009**, *201* (1), 93–99. DOI: <https://doi.org/10.1016/j.jmr.2009.08.004>
- [101] Z. I. Cleveland, H. E. Möller, L. W. Hedlund, B. Driehuis, *J. Phys. Chem. B.* **2009**, *113* (37), 12489–12499. DOI: <https://doi.org/10.1021/jp9049582>
- [102] J. Yang, P. Wang, J. G. Korvink, J. J. Brandner, S. Lehmkuhl, *ChemPhysChem* **2023**, e202300204. DOI: <https://doi.org/10.1002/cphc.202300204>
- [103] N. Kockmann, T. Kiefer, M. Engler, P. Woias, *Sensors Actuators B Chem.* **2006**, *117* (2), 495–508. DOI: <https://doi.org/10.1016/j.snb.2006.01.004>

- [104] J. Charpentier, *Chem. Eng. Technol.* **2005**, *28* (3), 255–258.
- [105] T. Nguyen, E. W. Byrd, D. Bentz, J. Martin, *J. Adhes.* **2005**, *81* (1), 1–28.
- [106] M. Bayareh, M. N. Ashani, A. Usefian, *Chem. Eng. Process.* **2020**, *147*, 107771. DOI: <https://doi.org/10.1016/j.cep.2019.107771>
- [107] S. G. Kandlikar, S. Colin, Y. Peles, S. Garimella, R. F. Pease, J. J. Brandner, D. B. Tuckerman, *J. Heat Transfer* **2013**, *135* (9), 091001. DOI: <https://doi.org/10.1115/1.4024354>
- [108] J. Yue, J. C. Schouten, T. A. Nijhuis, *Ind. Eng. Chem. Res.* **2012**, *51* (45), 14583–14609. DOI: <https://doi.org/10.1021/ie301258j>
- [109] B. A. Rizkin, F. G. Popovic, R. L. Hartman, *J. Vac. Sci. Technol., A* **2019**, *37* (5), 50801.
- [110] E. J. Tozzi, L. A. Bacca, W. H. Hartt, M. J. McCarthy, K. L. McCarthy, *Chem. Eng. Sci.* **2013**, *93*, 140–149. DOI: <https://doi.org/10.1016/j.ces.2013.02.007>
- [111] O. Mihailova, V. Lim, M. J. McCarthy, K. L. McCarthy, S. Bakalis, *Chem. Eng. Sci.* **2015**, *137*, 1014–1023. DOI: <https://doi.org/10.1016/j.ces.2015.07.015>
- [112] H. Herold, E. H. Hardy, A. Brodhagen, C. Müller, N. Nestle, *Chem. Eng. Sci.* **2015**, *134*, 599–604. DOI: <https://doi.org/10.1016/j.ces.2015.05.015>
- [113] S. Ahola, V.-V. Telkki, S. Stapf, *Lab Chip* **2012**, *12* (10), 1823. DOI: <https://doi.org/10.1039/c2lc21214e>
- [114] V. Lim, A. M. Hobby, M. J. McCarthy, K. L. McCarthy, *Chem. Eng. Sci.* **2015**, *137*, 1024–1033. DOI: <https://doi.org/10.1016/j.ces.2015.07.003>
- [115] M. Wiese, S. Benders, B. Blümich, M. Wessling, *Chem. Eng. J.* **2018**, *343*, 54–60. DOI: <https://doi.org/10.1016/j.ces.2018.02.096>
- [116] M. Plata, W. Hale, M. Sharma, J. M. Werner, M. Utz, *Lab Chip* **2021**, *21* (8), 1598–1603. DOI: <https://doi.org/10.1039/D0LC01100B>
- [117] M. Bornemann, S. Kern, N. Jurtz, T. Thiede, M. Kraume, M. Maiwald, *Ind. Eng. Chem. Res.* **2019**, *58* (42), 19562–19570. DOI: <https://doi.org/10.1021/acs.iecr.9b03746>
- [118] K. C. H. Tijssen, B. J. A. Van Weerdenburg, H. Zhang, J. W. G. Janssen, M. C. Feiters, P. J. M. Van Bentum, A. P. M. Kentgens, *Anal. Chem.* **2019**, *91* (20), 12636–12643. DOI: <https://doi.org/10.1021/acs.analchem.9b00895>
- [119] J. Ulpts, W. Dreher, L. Kiewidt, M. Schubert, J. Thöming, *Catal. Today.* **2016**, *273*, 91–98. DOI: <https://doi.org/10.1016/j.cattod.2016.02.062>
- [120] E. L. Sesti, J. Cui, S. E. Hayes, M. S. Conradi, *J. Magn. Reson.* **2017**, *282*, 136–141. DOI: <https://doi.org/10.1016/j.jmr.2017.08.005>
- [121] A. Brächer, S. Hoch, K. Albert, H. J. Kost, B. Werner, E. Von Harbou, H. Hasse, *J. Magn. Reson.* **2014**, *242*, 155–161. DOI: <https://doi.org/10.1016/j.jmr.2014.02.013>
- [122] A. Brächer, R. Behrens, E. von Harbou, H. Hasse, *Chem. Eng. J.* **2016**, *306*, 413–421. DOI: <https://doi.org/10.1016/j.ces.2016.07.045>
- [123] A. Hurtado, F. Loeffler, E. Bucharsky, K. Schell, E. Thompson, N. Nestle, H. Schreyer, J. Korvink, J. Brandner, *Chem. Eng. Trans.* **2021**, *86*, 1195–1200.
- [124] S.-T. Yang, *Bioprocessing for Value-Added Products from Renewable Resources: New Technologies and Applications*, Elsevier, Amsterdam **2011**.
- [125] N. Qin, P. Zhao, E. A. Ho, G. Xin, C. L. Ren, *ACS Sensors* **2020**, *6* (1), 3–21.
- [126] H. M. Wu, T. A. Lee, P. L. Ko, H. J. Chiang, C. C. Peng, Y. C. Tung, *J. Micromech. Microeng.* **2018**, *28* (4), 43001.
- [127] L. A. Low, C. Mummery, B. R. Berridge, C. P. Austin, D. A. Tagle, *Nat. Rev. Drug Discov.* **2021**, *20* (5), 345–361.
- [128] R. G. Willaert, K. Goossens, *Fermentation* **2015**, *1* (1), 38–78.
- [129] T. L. Palama, I. Canard, G. J. P. Rautureau, C. Mirande, S. Chatellier, B. Elena-Herrmann, *Analyst* **2016**, *141* (15), 4558–4561.
- [130] F. Delvigne, R. Takors, R. Mudde, W. van Gulik, H. Noorman, *Microb. Biotechnol.* **2017**, *10* (5), 1267–1274.
- [131] M. Jie, J.-M. Lin, *Cell Anal. Microfluid* **2018**, 339–370.
- [132] S. Halldorsson, E. Lucumi, R. Gómez-Sjöberg, R. M. T. Fleming, *Biosens. Bioelectron.* **2015**, *63*, 218–231.
- [133] J. Maisch, K. Kreppenhofers, S. Büchler, C. Merle, S. Sobich, B. Görling, B. Luy, R. Ahrens, A. E. Guber, P. Nick, *J. Plant Physiol.* **2016**, *200*, 28–34.
- [134] N. Mehendale, F. Jenne, C. Joshi, S. Sharma, S. K. Masakapalli, N. MacKinnon, *Molecules* **2020**, *25* (20), 4675.
- [135] J. Xue, N. G. Isern, R. J. Ewing, A. V. Liyu, J. A. Sears, H. Knapp, J. Iversen, D. R. Sisk, B. K. Ahring, P. D. Majors, *Appl. Microbiol. Biotechnol.* **2014**, *98*, 8367–8375.
- [136] D. Hertig, S. Maddah, R. Memedovski, S. Kurth, A. Moreno, M. Pennestri, A. Felser, J.-M. Nuoffer, P. Vermathen, *Analyst* **2021**, *146* (13), 4326–4339.
- [137] I. Alshamleh, N. Krause, C. Richter, N. Kurrle, H. Serve, U. L. Günther, H. Schwalbe, *Angew. Chem.* **2020**, *132* (6), 2324–2328.
- [138] H. Wen, Y. J. An, W. J. Xu, K. W. Kang, S. Park, *Angew. Chem., Int. Ed.* **2015**, *54* (18), 5374–5377.
- [139] A. Yilmaz, M. Utz, *Lab Chip* **2016**, *16* (11), 2079–2085.
- [140] B. Patra, M. Sharma, W. Hale, M. Utz, *Sci. Rep.* **2021**, *11* (1), 53.
- [141] E. Montinaro, M. Grisi, M. C. Letizia, L. Pethö, M. A. M. Gijs, R. Guidetti, J. Michler, J. Brugger, G. Boero, *PLoS One* **2018**, *13* (5), e0192780. DOI: <https://doi.org/10.1371/journal.pone.0192780>
- [142] T. Finkbeiner, C. Manz, M. L. Raorane, C. Metzger, L. Schmidt-Speicher, N. Shen, R. Ahrens, J. Maisch, P. Nick, A. E. Guber, *Protoplasma* **2022**, *259* (1), 173–186.
- [143] Z. I. Cleveland, H. E. Möller, L. W. Hedlund, J. C. Nouls, M. S. Freeman, Y. Qi, B. Driehuis, *PLoS One* **2012**, *7* (2), e31306.

DOI: 10.1002/cite.202300103

## Integrating Micro Process Chemistry into an NMR Spectrometer

Julia Schulte-Hermann, Jing Yang, Andrea C. Hurtado Rivera, Jan G. Korvink, Neil MacKinnon, Jürgen J. Brandner\*

**Review Article:** Miniaturization offers numerous opportunities in expanding the application space of NMR. These opportunities are reviewed in the context of the compatible materials and their manufacturing options, with particular focus on applications including micro process engineering, gas-based hyperpolarization, and small-scale bioreactors. ....

